AFRL-VS-TR-2001-1535

Measuring Electrodynamics of the Ionosphere by Digital Ionosondes and Other Techniques

B. Reinisch G. Sales

University of Massachusetts/Lowell
Center for Atmospheric Research
1 University Avenue
Lowell, MA 01854

20 July 2000

Scientific Report No. 1

APPROVED FOR PUBLIC RELEASE; DISTRIBUTION IS UNLIMITED.

20020520 171

AIR FORCE RESEARCH LABORATORY
Space Vehicles Directorate
29 Randolph Rd
AIR FORCE MATERIEL COMMAND
Hanscom AFB, MA 01731-3010

This technical report has been reviewed and is approved for publication.

B.S Dandekar
Balkrishna S. Dandekar
Contract Manager

Carl J. Christensen
Carl J. Christensen, Major, USAF
Acting Chief
Space Weather Center of Excellence

Qualified requestors may obtain additional copies form the Defense Technical Information Center (DTIC). All others should apply to the National Technical Information Service.

If your address has changed, if you with to be removed from the mailing list, or if the addressee is no longer employed by your organization, please notify AFRL/VSIM, 29 Randolph Rd., Hanscom AFB, MA 01731-3010. This will assist us in maintaining a current mailing list.

Do not return copies of this report unless contractual obligations or notices on a specific document require that it be returned.

REPORT DOCUMENTATION PAGE	*Form Approved* *OMB No. 0704-01-0188*

1. REPORT DATE *(DD-MM-YYYY)*	**2. REPORT TYPE**	**3. DATES COVERED** *(From - To)*
20-07-2000	Scientific#1	24 Sept 96-23 Sept 97

4. TITLE AND SUBTITLE
Measuring Electrodynamics of the Ionosphere by Digital Ionosondes and Other HF Techniques

5a. CONTRACT NUMBER
F19628-96-C-0159

5b. GRANT NUMBER

5c. PROGRAM ELEMENT NUMBER
62601F

6. AUTHORS
Bodo Reinisch, Gary Sales

5d. PROJECT NUMBER
1010

5e. TASK NUMBER
IC

5f. WORK UNIT NUMBER
AA

7. PERFORMING ORGANIZATION NAME(S) AND ADDRESS(ES)
University of Massachusetts Lowell
Center for Atmospheric Research
600 Suffolk St.
Lowell, MA 01854

8. PERFORMING ORGANIZATION REPORT NUMBER

9. SPONSORING/MONITORING AGENCY NAME(S) AND ADDRESS(ES)
Air Force Research Laboratory
29 Randolph Rd
Hanscom AFB, MA 01731-3010
Contract Manager: Balkrishna S. Dandekar, VSBXI

10. SPONSOR/MONITOR'S ACRONYM(S)

11. SPONSOR/MONITOR'S REPORT NUMBER(S)
AFRL-VS-TR-2001-1535

12. DISTRIBUTION/AVAILABILITY STATEMENT
Approved for public release; distribution unlimited

13. SUPPLEMENTARY NOTES

14. ABSTRACT
Extensive modeling of equatorial depletions was carried to compare the Agua Verde, Chile all-sky airglow (630.0 nm) observations with the Digisonde results from same site. The motion/structure of depletions observed away from magnetic equator showed west-to-east drift speeds of 80-100 m/s and lifetimes of the order of 2 hrs. On the quiet nights the airglow emission was about a factor of two greater than on nights when depletions were present indicating a lower F-layer altitude on quiet nights. This is consistent with the lack of depletions on the quiet nights as instabilities are more likely to form as altitude of layer increases. Qaanaaq polar Digisonde drift measurements were used to analyze the motion/structure of polar patches as they drifted over the site. A switch in IMF from Bz negative to positive resulted in the absence of patches after the change in field direction. Doppler analysis was used to separate the vertical ionosphere motion resulting from electron-ion recombination from the true vertical plasma drift. Results of this modeling are shown and Digisonde data from Puerto Rico are compared to incoherent scatter radar velocities.

15. SUBJECT TERMS
Ionosphere, equatorial scintillation, polar patches, Digisonde

16. SECURITY CLASSIFICATION OF: a. REPORT	b. ABSTRACT	c. THIS PAGE	**17. LIMITATION OF ABSTRACT**	**18. NUMBER OF PAGES**	**19a. NAME OF RESPONSIBLE PERSON**
UNCL	UNCL	UNCL	UNL		Balkrishna S. Dandekar
					19B. TELEPHONE NUMBER *(Include area code)* (781) 377-2761

Standard Form 298 (Rev. 8/98)
Prescribed by ANSI Std. Z39.18

CONTENTS

1. INTRODUCTION 1

2. RESEARCH 2

2.1 STRUCTURE OF EQUATORIAL IONOSPHERE 2

2.1.1 Equatorial Depletion Analysis 2

2.1.2 Equatorial Spread-F 7

2.2 POLAR CAP MONITORING 9

2.2.1 IMF Bz and By Polarity 9

2.3 DRIFT ANALYSIS TECHNIQUES 10

2.3.1 Doppler Analysis 10

2.3.2 Generalized Digisonde Drift Analysis 14

2.4 DIGISONDE DATABASE 15

2.4.1 Standardizing the Digisonde Drift Database Format 15

2.4.2 Maintenance of VIM Database 17

2.4.3 Archiving the Digisonde Database 18

2.4.4 Development of Internet Access of SAO Data Sets from Digisonde Stations 18

2.5 DIGISONDE NETWORK SUPPORT 19

2.5.1 ARTIST Upgrades 19

2.5.2 DISS Network Support 21

2.6 LOW POWER DIGITAL PORTABLE SOUNDER 21

2.7 DIGITAL SOUNDER FOR TOPSIDE OBSERVATIONS 23

2.7.1 Circuit Design 24

2.7.2 Waveform Development for TOPAS, Topside Advanced Sounder 25

2.7.3 Proposed Chirp Waveform Parameters 26

2.7.4 Synthesizer Card Design Modifications for Chirp Signal Generation 27

2.7.5 Software Modification to Existing DPS Code Required for a Chirp Waveform 28

2.7.6 Hardware/Firmware Modifications to DPS Design Required for Chirp Waveform . 29

2.7.7 Transmitted Power Calculations for 5W TOPAS Transmitters 33

3. PUBLICATIONS 33

4. SUMMARY 34

1. Introduction

The University of Massachusetts Lowell Center for Atmospheric Research (UMLCAR) continues to work for a better understanding of the physics of the upper atmosphere that can lead to reliable transionospheric and subionospheric communications meeting the needs of the United States Air Force. With the arrival of networking and super communication highways, space science has been propelled into real-time forecasting. New capabilities that can greatly enhance the ability of the United States Air Force to determine when communication systems may be affected by ionospheric and/or solar-terrestrial phenomena are being pursued at UMLCAR in conjunction with other institutions as part of the "Space Weather Forecasting" initiative.

The task of specifying the ionosphere has been subdivided into several areas. These include:

- **Structure of Equatorial Depletion Bands:**
  The plan is to study the morphology of equatorial depletions and to determine the physical cause for their development and behavior. Particular emphasis will be placed on the use of ionosonde and other high frequency (HF) measuring techniques involving both the experimental and theoretical investigation of these phenomena. The experimental part consists of measurements made with a variety of instruments during the campaigns planned by Air Force Research Laboratory (AFRL) scientists as well as using the routine observations at established equatorial sites such as at Jicamarca, Peru.

- **Polar Cap Monitoring:**
  Ionospheric drift measurements from high latitude Digital Ionospheric Sounding System (DISS) stations have shown a correlation between the sign of Bz and the plasma drift velocity. Ionospheric drift data from digital ionosondes at Qaanaaq, Greenland, SondreStromfjord, Greenland, Svalbard, Norway, and Goose Bay, Labrador are used to refine the process of determining polarity of Bz from ground-based ionospheric drift measurements. These results are used to develop the polar cap convection patterns.

- **Ionospheric Modification Diagnostics:**
  Under this task, UMLCAR is responsible for deploying the ionospheric diagnostic equipment, conducting measurements and providing quick-look data for the conduct of ionospheric heating experiments and analysis. UMLCAR also provides geophysical interpretation of the data.

- **Field Campaigns:**
  Under this task UMLCAR participates in measurements at remote field locations. UMLCAR provides support to PL in making joint measurements with other sensors using the DPS systems. As part of this task, UMLCAR will construct one four-receiver Digisonde Portable Sounder (DPS-4) system with four receive antennas.

- **Development of Digisonde Database:**
  UMLCAR collects and provides quality control on electron density profile data for selected periods and locations. These refined data are used to compare with the Air Force Research Laboratory's (AFRL's) Parametrized Ionospheric Model (PIM). Also,

UMLCAR is developing a standard format for these analyzed Digisonde drift data and archives these data in the Digisonde database.

- **Digisonde Network Support:**
UMLCAR provides upgrading of Digital Ionospheric Sounding System (DISS), AN/FMQ-12 and network support, particularly for building the ionospheric model database.

- **Low Power Digital Portable Sounder (LPD):**
UMLCAR is developing a prototype of a Low Power Digital Ionosonde needed for routing ionospheric measurements.

- **Topside automated Sounder, TOPAS:**
Under this task, UMLCAR is designing and building a compact and efficient prototype ionosonde for satellite-based observations.

2. Research

2.1 Structure of the Equatorial Ionosphere

2.1.1 Equatorial Depletion Analysis

Equatorial depletion bands are observed in the region north and south of the magnetic equator using optical imaging, particularly the 630.0 nm atomic oxygen emission. The presence of these bands has been correlated with the occurrence of satellite scintillation phenomena after sunset in the same region. These dark bands, resulting from a depleted electron density, are observed to move from west to east away from the sunset terminator. This effort is directed at understanding the structure and dynamics of these depletion bands using HF sounding techniques.

As part of this effort, radio and optical observations of the structural characteristics of the observed bands from the Multi Instrumented Studies of Equatorial Thermosphere Aeronomy (MISETA) campaign at Aqua Verde, Chile in September/October 1994 have been analyzed. The technique involves the scaling of the 630.0 nm optical all-sky image data and producing a time history of the width, depth and east/west velocity of the several depletions observed on 1 and 3 October 1994 for several hours after sunset. An electron density model of the depletion region was developed that was used with ray tracing as part of the effort to correlate the HF sounding data with optical data. This 3-D model of the depletion was used to calculate the expected 630.0 nm emission intensity and compare it with the observations. These results are also used to develop an improved model of the structure of these depletion bands.

A technique developed by R. Sheehan (unpublished) to calculate the vertical emission intensity was extended in order to calculate the entire all-sky image including the effects of a depletion band in the vicinity of the observation site. One problem that arose from this analysis was the conversion of the digitized optical data to emission intensity measured in Rayleighs (R). After several discussions with P. Ning of Keo Consultants, the company that built the High Frequency Active Auroral Research Program (HAARP) imager, it was realized that there was a significant discrepancy between the observations and the calculated intensity using a model of

the background ionosphere (PIM was used for the background). The observations show that about 40 R was a typical bright region outside the depletions while the calculations seemed to show values as high as 400 R and typically around 100 to 200 R, depending on the neutral atmospheric model chosen. We investigated the sensitivity of these results to the neutral density models, quenching rates, charge exchange rates and the electron density profiles, at least before and after the depletions were present (it is not possible to measure an electron density profile while depletions are in the vicinity of the sounder because of the intense spread F during those times). We concluded that the emission intensity was relatively sensitive to the details of the electron density profile. After reviewing published papers by Solomon [Solomon, S.C., P.B. Hays, and V.J. Abreu, The auroral 6300A emission: Observation and Modeling, *J. Geophys. Res, 93* (A9), 9867-9882, 1988] and by Link [Link, R., and L.L. Cogger, A reexamination of the O I 6300A Nightglow, *J. Geophys. Res., 93* (A9), 9883-9892, 1988] (the Link paper was the source of Sheehan's work) we confirmed that most of the parameters used in our analysis were reasonable and only the electron density profiles might be further reviewed. We were able to model the observed emissions, of the order of 40 R, by relatively small changes in the electron density profile. In one case, the emission intensity of 40 R was achieved by reducing the electron density by 20% and increasing the altitude of the peak of the layer by 10 km.

The basic electron density depletion model developed for the simulation discussed above had six parameters that allowed one to vary the model to fit the observed all-sky emission intensity across the image. Conceptually, the optical all-sky image is divided into two parts. The first represents the background emission, that is where no depletion exists, and the second part is the variation over the depletion band. The model parameters first are adjusted to match the observed background emission, typically of the order of 40 R at Agua Verde. Then the other parameters are adjusted, first to match the width of the depletion and then the depth and steepness of the transition from background to the depletion minimum.

Unfortunately, in the first model developed for these depletions, the adjustable parameters were coupled and varying one often affected the others. Also some peculiar models resulted with some selected values of the parameters. For these reasons it was decided to generate a new model that avoided some of these issues. The new electron density model as a function of longitude and altitude, is:

$$N_e(z,L) = C(L)\, N_{e,o} \exp\left[-\left(\frac{z - zm(L)}{D(L)}\right)^2\right]$$

where the longitude L for the Chile site varies from 280 to 295 degrees east, and the parameters C, D and zm all vary with longitude as:

$$\exp\left[-\left(\left|\frac{L - L_o}{2F}\right|\right)^{2p}\right].$$

Here L_0 is the longitude of the center of the depletion, zm is the altitude of the maximum electron density within the depletion, C is the depletion factor, D is the scale height of the depletion, F is the width of the depletion, and p controls the steepness of the profile transition

from the background to depletion minimum. The calculations based on this model with p = 3 are presented in Figure 1 for electron density as a function of altitude and longitude.

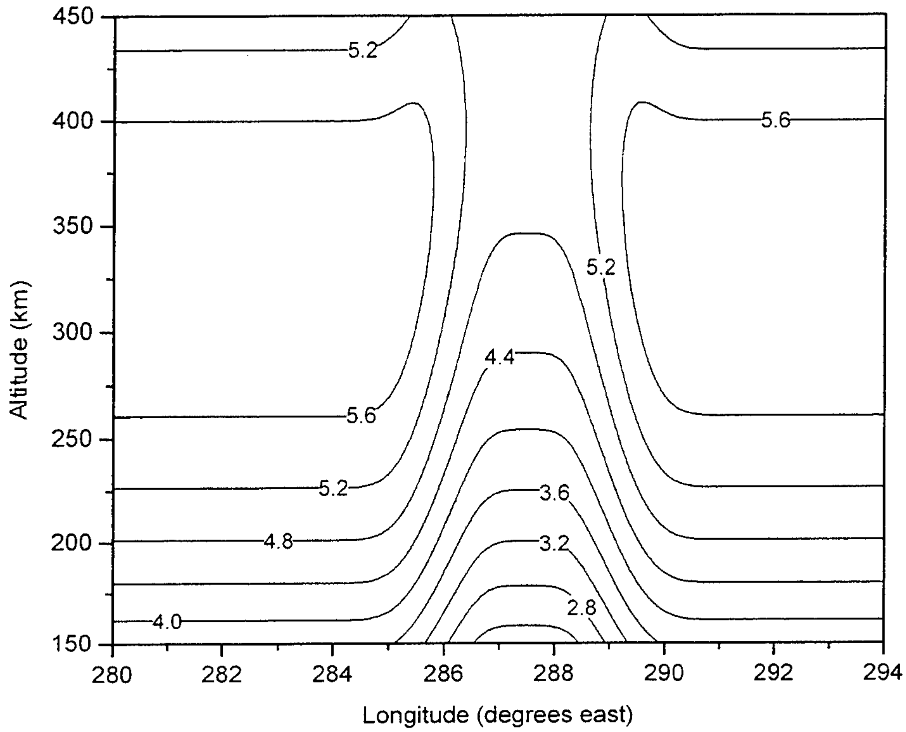

Figure 1. Depletion model (log electron density, cm^{-3}) vs. longitude.

The abscissa is the longitude (east), the ordinate is the altitude (km), and the contour labels are log (electron density – cm^{-3}). For this particular test case, the peak of the background F-layer is set at 330 km with a critical frequency of 8.3 MHz ($9x10^{11}m^{-3}$) while at the center of the depletion, the electron density peak is at 400 km and the critical frequency is 2.1 MHz ($0.5x10^{11}m^{-3}$). This new model is well behaved and it is now possible to compute the volumetric emission and the total emission that can be compared with the actual all-sky photometer data.

We undertook a statistical analysis of the MISETA images to determine the background and noise emission levels associated with the HAARP imager. The median of all pixels in the image was calculated, leaving out only the edges of the image that corresponds to the horizon region. The horizon was identified as the lowest 15 degrees that is usually contaminated with ground objects and mountains. The results showed median sky intensity at Agua Verde, Chile of about 40 R and a background noise level of 15 R. The noise level is particularly important in the analysis of the sky emission associated with the depletion bands, that is, to answer the question as to whether the minimum intensity inside the depletion band is noise or a low level of airglow. Our tentative conclusion is that even at the minimum of the depletion, some airglow is present and this directly affects the characteristics of the proposed depletion electron density model. Using these electron density models we were able to determine that the general

characteristics of the depletion do not change significantly as the depletion moves from west to east over the site. This may be a consequence of the age of the depletion and may not be true for depletions that have formed more recently.

The parametric depletion electron density model was used on the October 1994 MISETA campaign data in preparation for the upcoming paper to be delivered at the Montreal International Union of Radio Science (URSI) meeting. The new model worked well in generating electron density profiles within the two main depletions observed on October 1, 1994. The results were not dissimilar from those found earlier, primarily supporting the observation that the depletions are remarkably stable when observed away from the magnetic equator. Another important result of the optical analysis was that it is possible to follow the two main depletions for almost three hours, well into the time when the background emission has fallen to a very low value. At these late times it is not possible to determine the optical emission within the depletion, the level being below what the system can detect.

A new technique was developed to process the optical images using intensity cuts from west to east across the center of the all-sky images. These crosscuts are stacked vertically in time (one minute apart). Two of these depletions were observed for more than 180 minutes. One of these depletions formed near the middle of the image and remained very narrow for its lifetime, only about 40 minutes. Finally one depletion was already in the eastern sky when the recording began at 0002 UT (just after F-layer sunset). Each crosscut is the average of seven west-east lines across the image to produce a smoother variation. A five point running average is also applied from west to east. This smoothed curve is then differentiated to determine the location of the minimum intensity, defining the center of the depletion. A second derivative is performed on the smoothed crosscut to find the inflection points on the sides of the depletion, the spacing between these inflection points is defined as the width of the depletion. All of this analysis was carried out after the optical pixels (measuring angle from the observing site) were converted to geographic location, assuming the emission originates at an altitude of 300 km.

The track position of the depletion minimum in kilometers relative to the overhead position is plotted against time for the first 140 minutes. The time cutoff is due to the very low background emission after 0220 UT. The SNR is too low to have confidence in the differentiation process. The plot of these depletion tracks is shown in Figure 2. The same plots for October 3, 1994, are shown in Figure 3. Three depletions are seen on both days, each with a very consistent pattern of motion. This sequence of measurements occurred over a period of 120 minutes.

The results of the analysis to date were reviewed critically to determine what is understood about these depletions and what still remains to be investigated. The conclusions involving the relatively stable structure of these depletions and the uniform west-to-east drift at about 90 m/s are valid. The width characterization is suspect because of the decreasing background emission over the two hours of observations during the October 1994 campaign. At this point the width does not seem to be a critical factor.

A method has been developed to describe the growth and decay phases of these depletions during their lifetime by comparing the variations of the minimum emission intensity to the general background emission. Periods of growth were observed for the each depletion, where growth is defined as when the minimum intensity decreases faster than the background

emission. For one of the depletions on October 1, 1994 (Figure 4), we see a period of decay when the minimum intensity decreases faster than the background emission, ending when the minimum intensity actually reaches the background level. The two major depletions during the night of October 1 (Figure 4) show only growth followed by a stable period when the minimum intensity variation follows the background changes, neither growing nor decaying. If a decay phase did occur it was not observed, possibly because the minimum intensity reached the detector threshold and then, shortly after, the background intensity became too weak to see further development of these depletions. A similar plot for October 3 is shown in Figure 5. The average speed on October 1 was 96 m/s while on October 3, the average speed was about 90 m/s. It should be noted that on October 2, no depletions were observed and this "quiet" day was used as a control for the other two days, in terms of the background emission level.

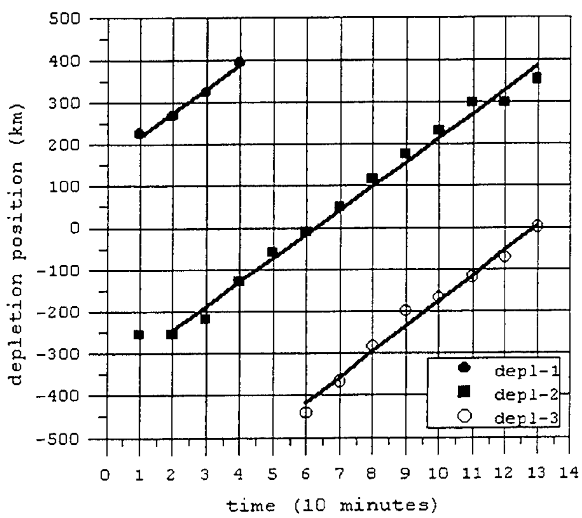

Figure 2. Measured depletion position vs. time after 00 UT after 00 UT on October 1, 1994.

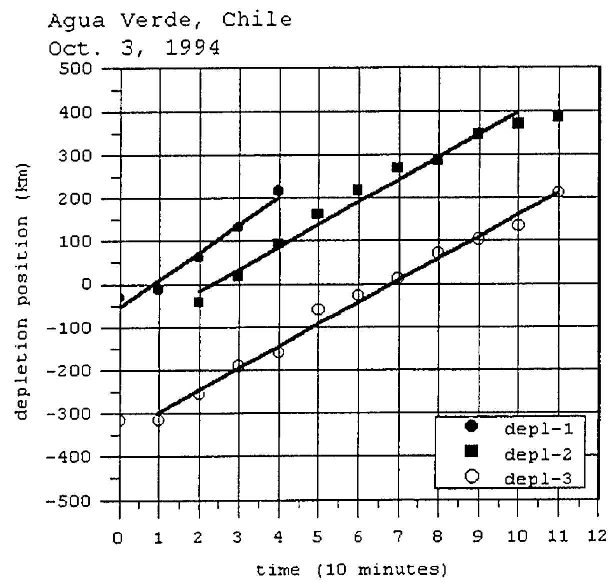

Figure 3. Measured depletion position vs. time after 00 UT on October 3, 1994.

The additional curve on Figures 4 and 5, indicated as "bkg", represents the background intensity, i.e., measurements taken in the areas of the image where no depletions are present. These background data were obtained by taking the median intensity within the largest area available on each image that did not contain a depletion. Here we see a rather steady background intensity until 0040 UT, followed by a 20% brightening and then, finally, a steady and rapid decrease in emission intensity as the lower F- layer begins to decay. It was estimated from these data that the minimum intensity detectable by the HAARP imager was about 15 R.

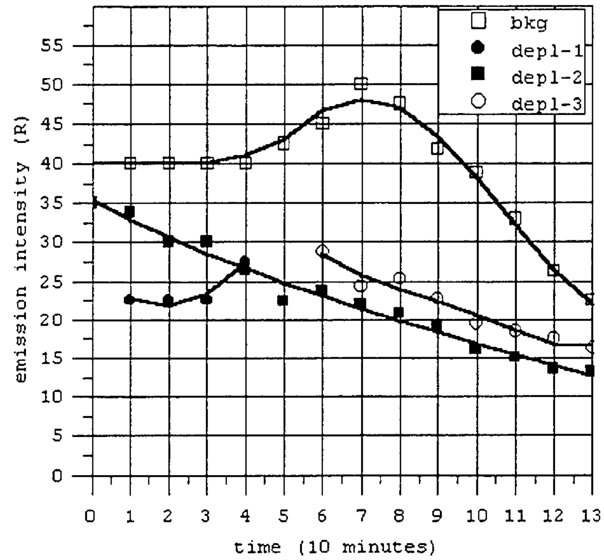

Figure 4. Depletion emission intensity on October 1, 1994, vs. time after 00 UT.

The behavior on October 3 of the background emission (bkg) is similar to what was observed on October 1, 1994 i.e., a relatively constant level of around 45R, at least until 0130 UT when the F-region decay reaches the point where the emission level begins to decrease. A distinct 20% brightening of the background emission is again observed, lasting 40 minutes, centered at 0030 UT, somewhat earlier than on October 1, 1994.

Finally, we looked at the background emission on October 2, 1994, a night when no depletions were observed. Figure 6 shows the variation of the background intensity over the two hours after sunset. Superimposed on the plot are the background intensities for the other two nights, October 1 and 3, 1994. The most obvious difference between the nights when depletions were observed (October 1 and 3) and October 2 is that on this night the emission intensity is a factor of two greater. On the basis of this rather limited data set, it is interesting that the ionospheres are so different on these different nights, correlating well with the presence or absence of depletions. Also the systematic nighttime decay begins some 20 to 30 minutes earlier on the "quiet" night.

2.1.2 Equatorial Spread-F

Satellite scintillation in the equatorial region is a serious problem after sunset. There is a need to predict with sufficient lead-time on which nights the scintillation will occur. In an effort to identify a triggering mechanism for the generation of instabilities that lead to the formation of spread-F irregularities, high time resolution ionogram data for Jicamarca were collected and scaled. In the routine mode of operation, the Digisonde at Jicamarca produces an ionogram only

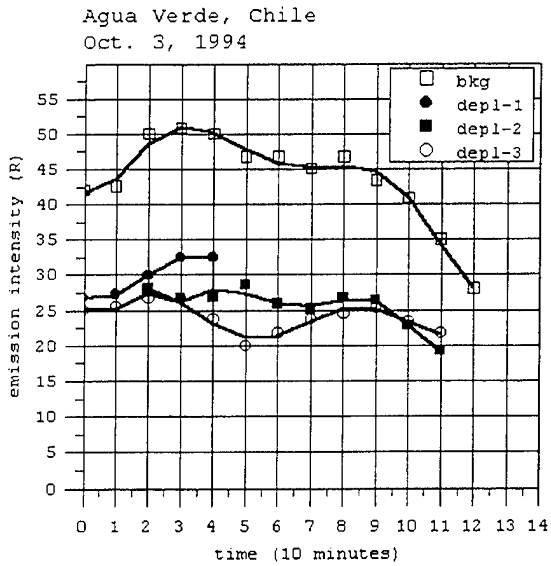

Figure 5. Depletion Emission Intensity on October 3. 1994 vs. time after 00 UT.

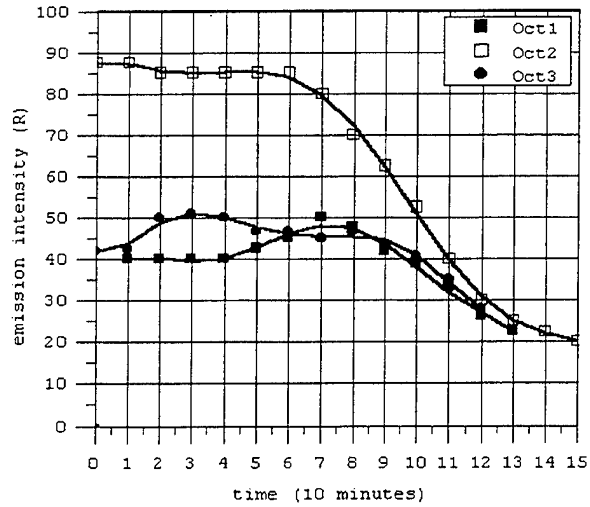

Figure 6. Comparison of the background emission levels during the MISETA campaign.

once every half-hour. This monitoring mode is too slow for the observations of short period gravity waves that can induce electric fields, resulting in the evening ionosphere being moved to greater heights. For this study, the Jicamarca Digisonde was operated in a four-minute ionogram mode for April 1, 2, and 4, 1997. These data were manually scaled to insure accurate results. While the campaign specifically requested that the Digisonde run four-minute ionograms, this mode was not maintained, and the Digisonde was switched back to the routine half-hour ionograms for at least seven hours each day. This unfortunately removed the ability to use a Fourier analysis to pull the different frequency components out of these data, especially since the loss of high resolution data occurred during daytime hours, at which time the conditions for the following nighttime were being established.

On the night of April 1-2, spread irregularities were not produced locally but drifted into the station field of view at around 0444 UT. On the other two nights, spread F signatures were observed immediately after sunset at around 0000 UT. As expected the lowest hmF2 was recorded on the night of April 1-2 when local spread-F irregularities were not produced.

Disregarding all the data loss due to inadequate system maintenance at Jicamarca during the requested Digisonde campaign, some positive observations were made that need to be pursued in order to forecast the occurrence of nighttime spread F from daytime signatures. The indirect measure of the equatorial E x B term may be made by observing the shape of the electron density contours at higher frequencies. This may be a good technique to determine if the conditions are optimal for nighttime spread F generation. It is clear from these observations that the most intense spread-F conditions occur when the E x B contour signature on the higher frequencies is small. This suggests:

a. Conditions exist where the fountain effect is not efficient in removing the ionization from the equatorial region, hence the foF2 increase to values larger

than normally observed, and the F-region layers remain at lower altitudes for longer periods of the day.

b. The increased level of ionization and the larger transition in altitude (dH/dt) at sunset set up optimal conditions for gradient instability mechanisms, which generate small-scale (<1 km) instabilities. The theory for the spontaneous generation of small instabilities for field-aligned irregularities at mid-latitudes (i.e. the gradient instability mechanism) states that the positive height gradient in plasma density must be large enough to compete with both collisional and recombination processes.

While this theory was developed for mid-latitudes, there does appear to be enough evidence from observations at Jicamarca to warrant its use in determining the effect of the large gradients in the equatorial regions.

This approach could provide a systematic procedure to understand the generation processes that could be involved. Gravity waves and the induced electric fields are very effective in terms of triggering the growth of instabilities, and the daytime conditions seem to be a good precursor in setting up the environment where gravity waves can trigger spread-F. This hypothesis used in earlier studies will be used with the statistical data sets collected at Jicamarca to determine if it is possible to use daytime characteristics to determine the onset of spread-F.

2.2 Polar Cap Monitoring

2.2.1 IMF B_z and B_y Polarity

The original data sets from Qaanaaq, Sondrestrom and Svalbard for the magnetic cloud event on 10 January 1997 were not complete. The full data sets have been collected and have been processed. In addition data sets from Goose Bay and Millstone Hill for the same time were collected and have been processed. The range of Digisonde stations from the polar region to the high- and mid-latitude regions provides the basis of an extended drift and electron density analysis for the response of the ionospheric conditions to the passage of the magnetic cloud.

Enhanced electron density structure (patch) events were identified from Qaanaaq datasheets from 20 to 30 March 1992. This data set was chosen since the IMF Bz component changed from negative to positive at the end of 29 March 1992, which was clearly observed in the Qaanaaq data by the lack of these enhancements on 30 March 1992. These data were processed with the Generalized Digisonde Drift Analysis (GDDA) to determine the extent of the deviation in the background velocity when such a patch moves over the station. The background electron density levels for a polar station at this time of year is evident from the foF2 values recorded on 30 March 1992, when Bz was positive and patches were not transported over Qaanaaq. On 30 March 1992 from 00 to 18 UT the F-layer critical frequency remained, on average, around 4 MHz. The increase from 4 to 10 MHz indicates the extent of the effects that patches have in modifying the structure in the ionosphere in the polar region.

These variations display height changes of almost 70 km within 15-minute intervals. This movement would require vertical ion motions of approximately 80 m/s. Recall that on 30 March 1992 no patches were observed to move over Qaanaaq, hence the height variations are due

purely to the movement of the background ionosphere. Discussions with Roger Smith (Univ. of Alaska) verified that large vertical winds, although not a common feature, are present in the polar region, and his analysis has shown winds of 100 to 150 m/s vertically at 89.3 deg. invariant latitudes. The suggested cause was heating of the auroral region.

2.3 Drift Analysis Techniques

2.3.1 Doppler Analysis

Based on the earlier work of Dr. Terence Bullett (Doctoral Thesis, Mid-Altitude Ionospheric Plasma Drift: A Comparison of Digital Ionosonde and Incoherent Scatter Radar Measurements at Millstone Hill, University of Massachusetts Lowell, Electrical Engineering Department, 1993) and Xueqin Huang (UMLCAR, personal communication), a new formulation of the problem of analyzing the DPS Doppler measurements for signals reflected from the F region was derived. It was assumed that the observed Doppler shifts combined two contributions, namely, chemical processes that remove or add electrons to the F region and vertical transport which transfers electrons either upward (positive velocity) or downward (negative velocity). Both of these processes modify the electron density profile which when integrated up to the reflection height yields the phase path; and then by differentiation with respect to time, the Doppler shift for a ground transmitted signal reflected from the ionosphere is obtained.

In the initial phase of this work, the simplifying assumption was made that the solar production of ionization was zero, appropriate after sunset. The other assumption introduced was that the vertical transport velocity is uniform over the height extent of the F region. This analysis was then used, first, to derive a sequence of electron density models indicating how these models change under these conditions after sunset, and then the expected values for the Doppler shifts were calculated as a function of frequency. With the assumption of a uniform vertical transport velocity, it is apparent that if the chemistry rate constants for charge exchange and recombination are known, then it should be possible to determine the required vertical velocity that best fits the observed Doppler shifts. This technique requires only the measured electron density profile obtained by inversion from the vertical ionogram and the measured Doppler shifts as a function of sounding frequency. The preliminary simulations were encouraging and we have now proceeded to test this new technique on actual data using 1994 data from the Ramey Digisonde.

The analysis of observed Doppler motions concentrated on the sounder data from the magnetic conjugate experiment of January 1994, first, on the Ramey (Puerto Rico) data. A new program was developed that uses two electron density profiles, separated in this case by 10 minutes, and derives the Doppler frequency shift from the difference in the profiles at the reflection altitude for selected frequencies. The expected Doppler frequency shift for frequencies from 2 MHz to 5 MHz in 1/2 megahertz steps were calculated (Figure 7). The lower portion of the two profiles is less reliable than the other parts of the profile and the 2 MHz data are not reliable. The reflection heights at these frequencies are shown in the figure below as circles superimposed on one of the profiles. The ordinate is the altitude in kilometers and the abscissa is the log of the electron density. Also shown are the reflection heights for frequencies from 2 to 4.5 MHz.

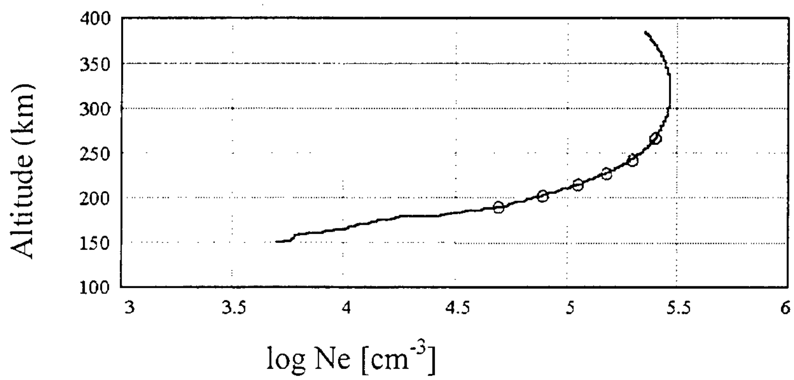

Figure 7. Electron density profile with reflection altitude for 2 to 4.5 MHz in 0.5 MHz steps.

For this profile, the calculated Doppler shifts are shown in Figure 8. The Doppler shifts are all positive, indicating the downward growth of the profiles during the 10 minutes around 0129 UT. The Ramey sounder, in the drift mode, made measurements at 2.445 MHz at that time and the mean Doppler shift was 0.066 Hz. This point (solid black circle) is plotted on the Doppler plot. The agreement between the calculated Doppler shift, using the motion of the reflection altitude, and the direct Doppler measurement is very good.

Using the theory for separating the chemistry and transport contributions to the observed Doppler, a program called "analytdop" was developed. The analytdop program calculates the expected Doppler shift from the chemistry and transport integrals where these integrals have to be evaluated at the upper limit, the reflection altitude. MATHCAD has a problem with the reflection altitude since the denominator of the integrand goes to zero at that point. Modification to the program made it possible to integrate within 200 m of the reflection altitude. We have also modified analytdop to be able to move the electron density profile and/or the neutral density profile up or down any desired distance, correcting for scaling errors. In the case of these data from 28 January we ran the program moving the electron density profile up by 0 and 10 km and the neutral profile down by 0 and 10 km. The results are shown in Figure 9.

Here the upper curve is +10 km for the electron density and -10 km for the neutral density. The middle curves are for electron density, +10 km, and neutral density, 0 km, and electron density, 0 km, and neutral density, -10 km, and finally the lowest curve is for electron density, 0 km, and neutral density, 0 km. All of these models show that it is necessary to have increasing downward transport as the altitude decreases at lower sounding frequencies. This, of course, makes it possible to have an increasing electron density near the bottom of the layer where the chemistry is removing electrons relatively rapidly.

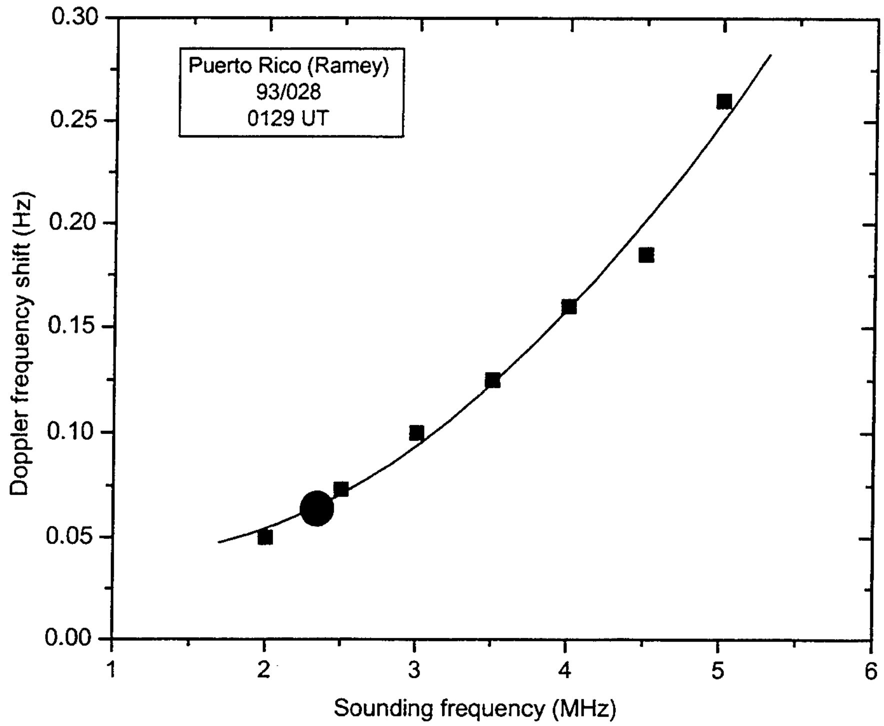

Figure 8. Doppler frequency as a function of sounding frequency. The solid line is a polynominal through the data points (squares).

For comparison with these results we have superimposed the incoherent scatter radar (ISR) measurements made at the same time at Arecibo. The ISR data points are the squares in Figure 9. From near the peak of the layer down to 225 km the agreement between the two measurements is good, assuming that the electron profile is moved up about 5 km and the neutral profile moved down by about the same amount. These are acceptable variations in the MSIS neutral profile and the electron density profile as measured by the Ramey sounder. To fit the ISR measurements at 200 km altitude, the profiles had to be shifted by 15 km in the same directions as before. Again, the question of the reliability of the bottom of the F-layer has to be addressed.

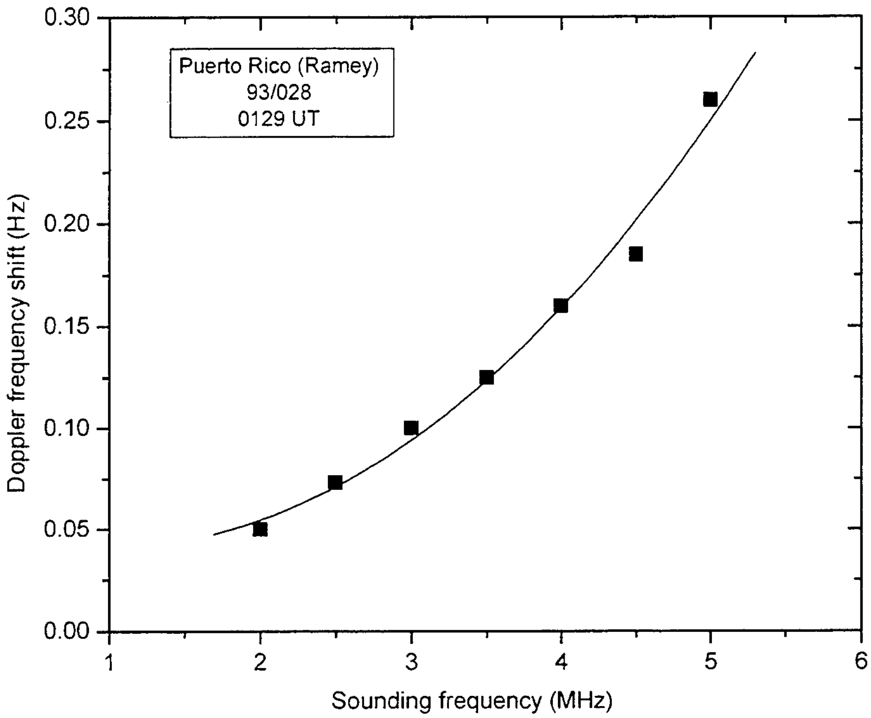

Figure 8. Doppler frequency as a function of sounding frequency. The solid line is a polynominal through the data points (squares).

For comparison with these results we have superimposed the incoherent scatter radar (ISR) measurements made at the same time at Arecibo. The ISR data points are the squares in Figure 9. From near the peak of the layer down to 225 km the agreement between the two measurements is good, assuming that the electron profile is moved up about 5 km and the neutral profile moved down by about the same amount. These are acceptable variations in the MSIS neutral profile and the electron density profile as measured by the Ramey sounder. To fit the ISR measurements at 200 km altitude, the profiles had to be shifted by 15 km in the same directions as before. Again, the question of the reliability of the bottom of the F-layer has to be addressed.

It was decided to also look at the Puerto Madryn (PM) data during the same conjugate experiment as the Puerto Rico (PR) data discussed above. Although the two sites are magnetically conjugate, it was felt that the PM data would be simpler to analyze because at the lower geographic latitude the station would not be bothered by the tidal waves that seem to affect PR during the evening hours. This will be investigated next year.

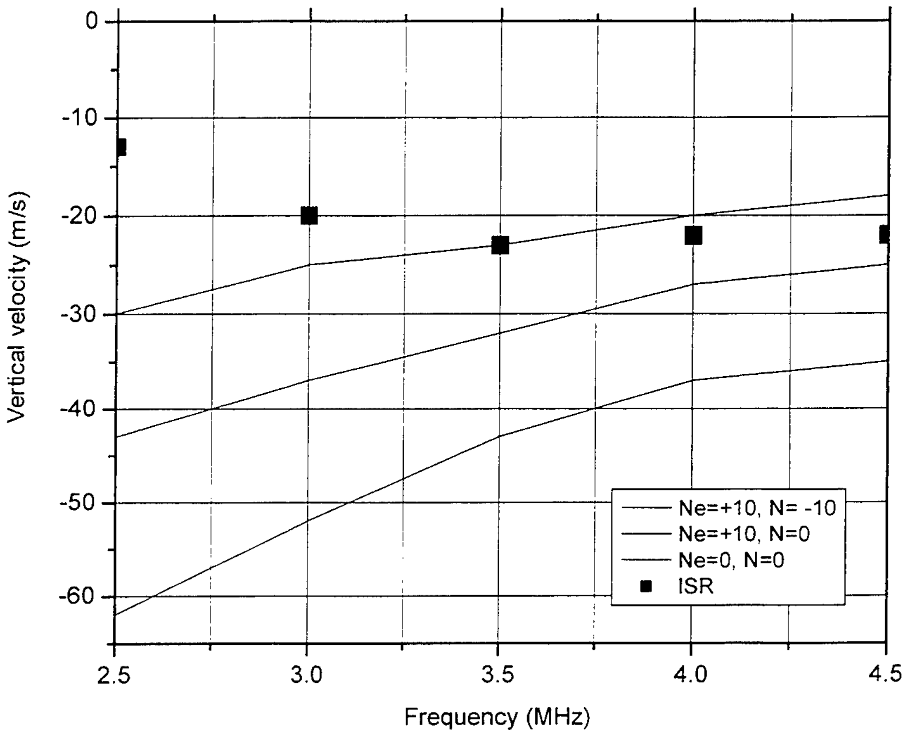

Figure 9. Vertical velocity vs. sounding frequency (reflection altitude) for Puerto Rico (Ramey) on 93/028 at 0129 UT.

2.3.2 Generalized Digisonde Drift Analysis

The Generalized Digisonde Drift Analysis (GDDA) method was developed to improve the drift analysis performance, particularly when the observation field is likely to contain a non-uniform drift pattern. This new method currently consumes a great amount of time in producing the velocity field, primarily because of the number of "sources" (recall that a source represents the location and Doppler of a reflection point) being identified in the skymap data. This can lead to 1,000,000 potential source combinations. To reduce the number of combinations requires a reduction of the number of "sources" identified. One reason for the large number of sources is the use of Hanning weighting, producing at least three spectral lines for each actual source in the drift spectra. Methods have been devised to solve this problem and reduce the processing time for GDDA that will make it more useful in a real-time processing environment.

Because of the need to transfer the Digisonde drift software to the Windows environment, the required improvements in the source detection algorithms needed for the new generalized

method and the compatibility with the Digisonde C/C++ libraries, the Digisonde programs have been converted to the C/C++ language. Currently functions for the least-squares fitting for a 2-dimensional and 3-dimensional antenna field have been completed and tested. The C/C++ GDDA program will be the first program to allow a 3-dimensional antenna field.

The DDA method can be used for a first pass on the velocity calculation. For large scale statistics the DDA method with smoothing would be sufficient. However for detailed interpretation of the rapid variations returned by DDA, the GDDA method "must" always be adopted. This is not just true for the Digisonde drift method, but is equally important for any velocity analysis technique, such as the ISR and SuperDarn systems. It is insufficient to return velocities estimated on averaged, smoothed, or fitted velocity data sets, imposed because of the limitations on the instrument, and/or velocity calculation scheme, especially when interpretation of electric field magnitudes are required.

In accordance with developing Digisonde drift applications that are platform independent, the GDDA application programs are being transferred and developed under the object oriented methodologies offered by the Java language. Currently the Digisonde Data-Passport object has been completed. This object allows the user to unpack all of the Digisonde data formats including the drift formats produced by the DGS-256 and DPS systems. This facilitates the use of Digisonde data sets that, due to different development stages and versions, can be quite complex in unpacking and interpreting. With the new Data passport object this is no longer a problem. The user just calls the required object and the data is automatically unpacked and made available. Now, using the Data Passport object, a preliminary working version of a Java GUI application to display DGS and DPS drift spectra has been developed. The program is called ShowSpectrum and incorporates the use of click and display buttons to navigate through Digisonde drift data sets. Text displays are also produced that contain specifics of the drift mode running, antenna configuration, and the actual data. The ShowSpectrum program serves as a quick display of the drift data and is a step towards the Java arsenal of diagnostic tools and objects from which the Java version of GDDA will be developed.

2.4 Digisonde Database

2.4.1 Standardizing the Digisonde Drift Database Format

The data generated by the DPS-1 at Jicamarca, Peru is stored on QIC cartridge tapes at the site. This year we have received cartridges from 001 (with data starting on 92080: March 20, 1992) to number 111 (containing data from 96302 to 96309: October 28, 1996 to November 04, 1996) with a gap of tapes 072 to 079 (95159 to 95264: June 08, 1995 to September 21, 1995). Cartridges 001 to 050 (up to 94255: September 12, 1995) contained mostly MMM, Artist, Drift and ION data types. The Jicamarca DPS was updated after tape 50 with the capability of producing RSF data, so in subsequent cartridges the MMM format is replaced by the RSF format.

Archiving of cartridges 001 to 033 and 042 to 050 on CD-ROM was completed in the summer of 1995. Tapes 034 to 041 (94033 to 94140: February 2, 1994 to May 20, 1994) were not available at the time. The data format on CD-ROM consisted of one-day files combining Ionogram, ARTIST and Drift data (.MMM, .ART and .DFT -- .ION files are not archived) for a

single day into one file named according to the station and the date: for example, file JI92080.TAP contains data measured at Jicamarca on 92080; the .TAP extension indicates that it is TAPe data. One-day disk files were made from the data on tape using the Fortran program TXQ written by Terence W. Bullett of AFRL. Each CD-ROM includes as many one-day files as can be accommodated in the available 650 megabytes.

Later, we received the cartridges 034 to 041. In the fall of 1996, these were transferred to CD-ROMs but in a different file format. Each CD-ROM was divided into three sub-directories IONOGRAM, SCALINGS and DRIFT. The tape data were again combined into one-day groups, but keeping the different data types separate: the ionoGRaM files was given an extension of .GRM (e.g. JI94033.GRM); the ARTIST files, an extension of .ART; and the DriFT files, an extension of .DFT. The program used to combine the tape data was a C-language program TAPESCAN written by Ivan Galkin of UMLCAR. Each data type was put into its own sub-directory on the CD-ROM: .GRM into \IONOGRAM; .ART into \SCALINGS; and .DFT into \DRIFT.

As mentioned above, starting with cartridge 052 (number 051 contained only test data), the Jicamarca MMM ionograms were replaced with RSF ionograms. The so-called RSF-flex data type is written in files of varying lengths, as opposed to the standard DGS- and DPS-file size of multiples of 4096 bytes. The only data-analysis software that can handle this data type is ADEP. Initially, the RSF data on cartridge was merged into one-day files (given an extension .NST: Non-STandard, because of the non-standard flexible file size) using ADEP Library, which can write into one disk file all the data it reads from tape between the starting and ending dates/times manually specified. It was soon discovered however that ADEP is very sensitive to errors in the RSF files and often gets lost in reading cartridge data and cannot find the preface; or it can go into an endless loop, repeatedly writing out the same data over and over. It was then decided to restore the individual RSF ionograms to disk with program READQIC written by David Kitrosser of UMLCAR and then to combine them into one-day groups using DOS's copy/b command. ADEP is used to verify each one-day file; if ADEP hangs up, the ionogram time is noted and a new one-day .NST file is created excluding that ionogram. Sometimes the process has to be repeated, when it is the ionogram after the time when ADEP balked that is damaged. This trial and error method is time-consuming, but it is necessary for weeding out the ionograms that were not written correctly.

Another problem that was discovered is that the different ADEP functions are not necessarily all affected the same way by the tape errors. One set of data was edited (with ADEP Editor) directly from the cartridge. The same data were then run through ADEP Survey; error after error kept popping up. The ionograms and ARTIST files were then restored to disk and a Fortran program called FIX_RSF was written to examine them in detail. It was discovered that several ionograms included data that seemed extraneous: groups of 256 pairs of the numbers 32 (20 hex) and 8. FIX_RSF was modified to rewrite the ionograms without those numbers, and then ADEP Survey had no more problems with the ionograms. FIX_RSF also discovered that other ionograms that also made ADEP hang up had been truncated; using FIX_RSF to sort out those ionograms so that they can be excluded from the one-day files is faster than the method described above (running each file through ADEP to discover the errors). It is suspected that the truncated files cause ADEP to hang up mostly because the End-Of-Ionogram marker (Eh) is absent. FIX_RSF was modified to insert the marker when it is missing; this eliminates the

problem encountered by ADEP. Using FIX_RSF routinely was faster and more efficient for resolving the issue of corrupted data.

CD-ROM copies of the available 1996 data from Millstone Hill and Jicamarca were prepared for the World Data Center A (Ray Conkright). No drift data were available from Millstone Hill for that time period, so the two CD-ROMS included only the ionogram and ARTIST data. Even though the Jicamarca data included drift data, all the data fit onto one CD-ROM.

A report on the chosen format of the CD-ROM Digisonde archive had been finalized and was submitted to the Air Force. An additional change was made using the extended data filename format. This extended file name is supported by current operating systems, with some capability for uniqueness in the older OS that use only an 8-character filename and 3-character extension. The extended file name was supported by UMLCAR, and the World data centers in UK and Japan, and hopefully by the WDC in Boulder Colorado. The extended file name is transferable to CD-ROM using today's CD writing software. UMLCAR will keep projecting into the future and will not limit our database requirements to old out-dated and inflexible systems.

2.4.2 Maintenance of VIM Database

The Jicamarca ionograms were adjusted since all heights were in error. The scaled data set was input to NHPC.EXE where the virtual heights where increased by 11 km. This height correction is required at Jicamarca as shown with the help of PGH ionograms. The VIM database was expanded with an additional 1.5 months of scaled Wallops Island data, stored in the UMLDAT database. All data sets are being stored in the SAO ADEP output formats. Continuing along the same lines, in support of modeling effort at AFRL, ionograms from Eglin AFB and Bermuda for days 36, 40, 42, 45 and 47, 1997 were manually scaled and the electron density profiles supplied.

In addition the VIM database was expanded to include an additional three months of scaled Jicamarca data from April to June, 1997, housed in the UMLDAT database. All data sets are being stored in the SAO ADEP output formats. Jicamarca ionograms are being regularly scaled starting from June, 1997 and working backwards. Monthly plots of electron density profiles, monthly averaged parameters for geomagnetically quiet and disturbed conditions are being produced, as well as dH/dt monthly plots for spread and no-spread conditions.

Finally, for this year the VIM database has an additional 12 months of scaled Jicamarca data from June 1996 to June 1997, housed in the UMLDAT database. All data sets are being stored in the SAO 3.0 output formats. New Jicamarca ionograms starting in 1992 are being regularly scaled. Monthly plots of electron density profiles, monthly averaged parameters for geomagnetically quiet and disturbed conditions will be produced, as well as dH/dt monthly plots for spread and no spread conditions. The aim is to provide enough quality data to produce the statistical analysis required to identify daytime signatures that can be used to forecast spread-F conditions, and a firm database for further modeling efforts.

2.4.3 Archiving the Digisonde Database

The archiving of Millstone Hill data on CD-ROMs has continued. The ionogram, ARTIST and drift data up to 97346 (Dec 12, 1997) at Millstone have been archived. Each CD-ROM is created when the accumulated data approaches about 630 to 650 million bytes. A CD-ROM can in principle hold 650 Mb but some of the space on the CD is needed for directory names, table of contents, etc.

The CD's are not rewriteable, so the data files are checked thoroughly before the CD is written. The data of an entire day's measurements are combined into 3 one-day files: an ionogram file, an ARTIST/scaling file and a drift file. The one-day files are then processed with ADEP to make sure that ADEP will not fail on errors in the data. ADEP does occasionally encounter data that it can neither interpret nor skip; in that case the file in question is checked more carefully to determine which part of the data causes the problem, and the data are fixed or one or more blocks of data are removed. The completed one-day files are also processed with Fortran program PrefDT.exe (Preface/Date/Time) that lists to an output file the record number, date and time of each record of data. This verifies that the data are readable. The resulting output file is later compared with similar outputs from the data files copied on the CD-ROMs, to verify that the CD copies are identical to the original files. Then 2 CD-ROM copies are made (the 2nd one is a backup, in case the first one is lost or damaged). It is not unusual that a CD-writing session is aborted by errors that are difficult to identify, so another CD must be generated. At times, in reading the data with the Fortran program, it was discovered that not all the data on a CD are accessible, so a new one was created. Sometimes, data that are readable on one CD reader cannot be read on another CD reader (the CD is consistently readable on one computer and consistently unreadable on the other), so it is never possible to be sure that a given CD will be readable on all computers.

Cartridge data from Tromso for the period of December 1996 to January 1997 contained many errors and had to be analyzed in detail and corrected. Much of the data could not be restored from the tapes with the normal utilities such as RT.COM and READQIC.COM. To access that data, the utility TAPEX.COM had to be used to advance the tape beyond the data errors that blocked up READQIC. This was a very time-consuming process because when the tape was advanced too far (it was very difficult to judge how much to advance it) it couldn't be backed up by a specific number of blocks but had to be rewound to the very beginning and then the process would be started all over. Using this procedure, three CD-ROMs were made with Tromso data covering the time period 96336 to 97013 (Dec 1, 1996 to Jan 13, 1997).

2.4.4 Development of Internet access of SAO data sets from Digisonde Stations

Using the Common Gateway Interface "CGI" architecture a proposal and preliminary design for providing Digisonde SAO data sets was developed. The basic setup as illustrated in Figure 10 uses the concept of a thin client being serviced by a data retrieval engine operating as part of the CGI system. In order to provide this type of Internet access to Digisonde SAO data sets, a flat file database system was designed for the back end. The design was adopted from previous Data center file/directory setup.

Data sets from the Digisondes will eventually be accessible (under specific security restrictions) to the ionospheric community supporting and improving the models and near/far forecasting capabilities. The front-end implementation will be via Java Applet Digisonde_OL.class, while the back end engine Dbscan.exe will be developed in C++.

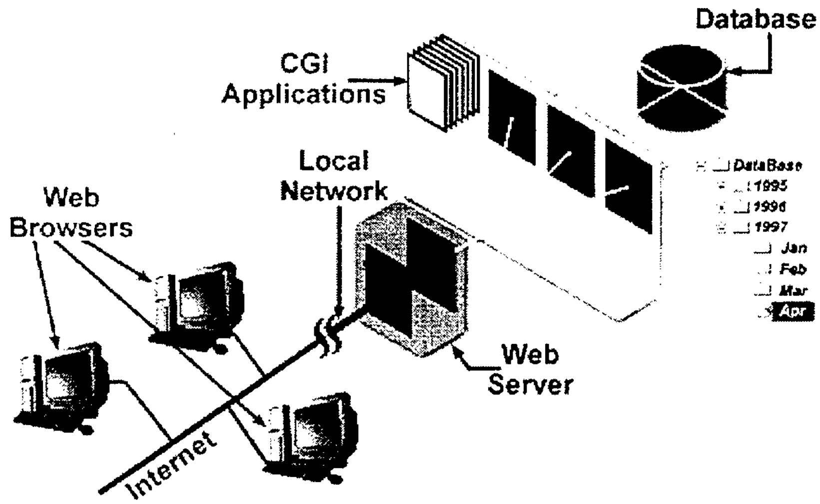

Figure 10. Basic internet access to SAO files.

2.5 Digisonde Network Support

2.5.1 ARTIST Upgrades

The new software, ARTIST4, was developed for DPS application. Design and testing has been completed for application of ARTIST4 to DGS256 systems. This was done by adding a new computer to the system for running ARTIST4, data storage and data delivery through the Internet. The original computer for the DGS256 system does not carry out the task of automatic scaling any longer but delivers data to the new ARTIST4 computer. With regard to the software, a new program DARTIST3 (Dummy ARTIST3) has been developed which accomplishes the following tasks:

(1) Deliver the measured ionogram data file DateTime.MMM or DateTime.DFT to the ARTIST4 computer; (2) read the file DateTime.SAO from the ARTIST4 computer; (3) display the scaled ionogram on the screen and optionally print it; (4) send a frequency value to DGS256 system for autodrift mode measurement; and (5) DARTIST3 and ARTIST4 share the same ARMENU file. This means that any changes in the ARMENU file that are made either by the ARTIST3 or ARTIST4 computer will be transferred to the other computer to update that ARMENU file.

The DARTIST3 has all the functions of ARTIST3 but the automatic scaling is done by ARTIST4 in the new computer. The tests at Millstone Hill have successfully demonstrated the new design. Discussions with Dr. Terry Bullett (AFRL) were held concerning the design of the

upcoming ARTIST4 upgrade for the DISS network. Several systems were procured and were being set up for installation at Wallops Island, Sacramento, Vandenburg, and Dyess.

Specifications for ARTIST4/Phase1 hardware were developed as a result of these discussions with Dr. T. Bullett and studies done at SondreStromfjord, Greenland. These studies, in addition to being a complete Year 2000 (Y2K) study, also were an exercise to determine the configuration of the future USAF ARTIST4 upgrades to the DISS network. It was decided that the ARTIST4 computers should be 200 MHz Pentium computers with 32 megabytes of RAM. The hard disks were to be high quality SCSI drives, two per system; one installed, and one for a spare or for swapping with upgraded software later. These hard disks were to be mounted in removable, slide out, trays. Each ARTIST4 computer would have two Ethernet cards for isolating the Air Force lines or NIPRNET from an optional LAN or Internet connection. Data storage at the site would be on a 525 megabyte QIC tape drive. A separate serial I/O port card (rather than built in serial ports on the Pentium motherboard) would be used for connection to an external modem for an optional RAS connection so that possible lightning damage will likely be limited to the plug-in card rather than the motherboard itself.

This approach, requiring minimum development, keeps the original ARTIST3 computer as an interface to the Processor chassis Input and Output computer and as an interface to the "COMEDS" type leased line communications which would be necessary to continue with at some stations into 1999. Eventually, all of the communications would be over network connections using leased lines or the Air Force NIPRNET. The only hardware change to the ARTIST3 computers was the addition of an Ethernet card to allow the ARTIST3 to communicate with the ARTIST4. File sharing techniques using Microsoft NetBEUI protocol allows the ARTIST3 to execute off of a network drive, which was on the ARTIST4 after the network connection was established. One advantage of this configuration (executing off of a network drive on the ARTIST4) is that any software upgrade of the ARTIST3 (or ARTIST4) can be made over the NIPRNET or Internet. This software that executes on the ARTIST3 computer was a simple Microsoft DOS network client either installed on the hard disk or on a bootable floppy disk.

Experiments were carried out on PGP encryption techniques. A possible option, considered early in the ARTIST4 design process, was using encryption to prevent possible spoofing of data. In addition, a security model was designed that restricts access to any data newer than 3 days (for example) to those with a user name and password on the system. The local ARTIST4 data storage layout was reworked to provide authenticated access to the specified period of the latest ionospheric data. The filed patching scheme was extended to adopt secured and public data areas with raw data files, ionogram pictures, one-day raw data files and one day SAO files accessible via an HTTP layer. Security management was extended to allow for the proper authentication for FTP and www users accessing the ARTIST4 system. User groups were created with a set of distinct privileges. The housekeeping scheme was reworked to ensure proper release of restricted data into the public area and maintain a specified amount of free hard disk space in the public data areas.

A DISS HTML page was created to provide the necessary functionality for the categories of www users accessing sounders (AF-guests, AF-users, AF-administrators). CGI script routines are developed for dynamic access to the constantly changing contents of published data.

Finally a new feature was added to the ARTIST4 program to support ray-tracing projects and to estimate ionospheric refraction effects for transionospheric propagation. The output of all ARTIST4 data is now in the SAO 4.2 format. ARTIST4 was modified to calculate the electron density up to 1000 km altitude using a α-Chapman profile for the topside ionosphere. A suitable scale height is automatically determined from the bottomside F region profile based on empirical modeling. Comparison with incoherent scatter radar observations at Millstone Hill and Faraday data at Sagamore Hill has shown excellent agreement. For easier application by users, the electron density profile is tabulated as function of height up to 1000 km: f_N (h) and N(h). The tabulation stops when $f_N < 0.2$ MHz. The height increments are selectable in 1 km steps.

2.5.2 DISS Network Support

Supporting the USAF DISS network as well as other Digisonde sites involved visits to many locations during this year. The support includes repairs, consultations, calibrations and maintenance. The sites visited were:

RAF Fairford, UK
USAF AWS/Space Forecasting
Rutherford Appleton Laboratory, UK
SondreStromfjord, Greenland
Bermuda
Sacramento

2.6 Low Power Digital Portable Sounder

To support the USAF requirement for a low power ionospheric sounder, primarily for oblique communications, UMLCAR has begun a research program to identify the problems and to generate solutions. The investigation has identified signal processing as the most fruitful direction. This effort has focused on the following processing techniques but has also included redesign of the DPS hardware and software.

1. Spike Clipping - Using the oblique CW transmission mode of the DPS, we expect the signal to arrive with a constant envelope amplitude, therefore some improvement in received signal to noise ratio (SNR) can be achieved by eliminating impulsive amplitude bursts, e.g. such as noise bursts from lightning strikes. This technique, referred to as "spike clipping", was implemented by setting a threshold 12dB (factor of 4 in amplitude) higher than the average received signal, then linearly reducing both quadrature components of any samples that exceed this threshold. Scaling down both the real and imaginary components of the signal proportionally maintains the phase of the received signal.

2. 2-D Image Processing - The determination of a level representing the noise floor in the received signal is critical to the correct setting of a cleaning threshold, such that the display programs and automatic ionogram scaling programs eliminate height-frequency bins that contain only noise and interference. UMLCAR's previous algorithm selected the maximum amplitude Doppler line at each height-

frequency bin and then displayed only the bins that exceeded the most probable amplitude (MPA) by more than 6dB. The new algorithm makes a histogram of the entire two-dimensional array of range and Doppler bins before selecting the maximum Doppler lines, resulting in a much larger number of points in the histogram distribution and therefore a smoother function. The inclusion of all the noise floor samples in each Doppler spectrum guarantees that the MPA is really noise, whereas the previous algorithm could conclude, especially under range spreading (i.e. spread-F echoes) conditions, that the signal amplitude was the MPA and therefore the signal would be considered noise.

3. The selection of maximum amplitude in the Doppler spectrum is very critical, since from that point on the amplitude and phase for each height-frequency bin is represented by the amplitude and phase of the selected Doppler line. For vertical sounding, ignoring echoes that are not from a narrow cone of acceptance around the vertical reduces the possibility of missing the overhead echo. A 6dB advantage has been given to overhead echoes by first summing the echo samples from the 4 antennas before selecting a maximum Doppler line. This is equivalent to digitally forming an antenna beam directed vertically.

4. Adaptive Noise Cancellation of In-Band Interference - The DPS signal has a bandwidth of 30 kHz that is necessary in order to achieve a range resolution of 5 km. Within this bandwidth, up to six interfering single-sideband communications channels could be encountered. Each of these has been shown to typically occupy instantaneous frequency bandwidths as narrow as 100 Hz (Rogers, D.C., and B. J. Turner, MITRE Corporation, MTR 9625, March 1985). Therefore it is necessary to detect narrowband peaks within the bandwidth of the received signals by Fourier transforming each height record (the record of 128 or 256 samples taken after each transmitted pulse), computing the noise floor and eliminating any spectral peaks that stand more than 12dB above that noise floor in the manner described above for the "spike clipping" algorithm.

5. Another effort is to implement an optimum Kalman Filtering weighting technique to reduce non-DPS-like components of the received signal. Several discriminating features of the DPS signal can be used to estimate the probability that energy detected at any given height-frequency cell is actually echo signal. These include:

   a. Consistency of phase among the four antennas.

   b. Consistency of signal amplitude and phase at two adjacent heights (when sampling the 5 km wide pulse at 2.5 km sample spacing),

   c. Increase in amplitude after pulse compression vs. raw sample amplitude consistent with the expected pulse compression gain of 15dB,

   d. Consistency of amplitude and Doppler detected at two adjacent frequency steps,

e. Consistency of amplitude between the O polarized and X polarized reception of the same height-frequency bin. Actual signals will strongly favor only one polarization.

6. Minimum Redundancy Pulse Sequences. Techniques for optimum pulse spacing have been developed, and three spectral analysis techniques have been evaluated for their effectiveness in producing valid spectra. The challenge stems from the irregular sample spacing of the received echoes. Common Doppler integration using Fourier transforms requires that the time domain samples be evenly spaced. Therefore, we investigated:

   a. Periodograms - A Fourier transform of the autocorrelation function of the received signal samples.

   b. Maximum-Entropy Spectral Estimation - Solution of a linear prediction filter corresponding to the received signal samples.

   c. Iterative Fourier Analysis - Filling in the "missing samples" by inverse transformation of each successive forward transform, starting with the "missing samples" being set to zero.

The Maximum-Entropy technique gave the best reconstruction of the original input when tested with simulated data. It works best when the order of the prediction filter matches the number of spectral components in the data. Therefore, a combined technique is being considered where the periodogram is used to estimate the number of source lines, then Maximum-Entropy is used to produce the spectra.

Using the undersampling technique, we can examine the continuity of the frequency ramp created by the prototype of the Direct Digital Synthesizer for TOPAS. This ramp is made by incrementing the commanded frequency of the DDS chip (STEL-1173 from Stanford Telecomm) 32,000 times per second in steps of 312.5 Hz.

The real-time control software has been written in high-level language C and has been demonstrated in a modified Digisonde sounder chassis running on a 486 PC clone-ISA motherboard system. A TMS320C30 Digital Signal Processor (DSP) board, also installed in the ISA backplane, performs pulse compression and spectral integration and operates the digitizer. The 486 computer can address the DPS board to examine the digitizer samples, the pulse compression output and the logarithmically scaled results after spectral integration, thereby verifying the correct operation of the software.

2.7 Digital Ionosonde Topside Observations

Another area of interest to the USAF is the implementation of a new topside ionospheric sounding system. The Digisonde Portable Sounder (DPS) and the Radio Plasma Imager (RPI), both developed by UMLCAR, might serve as prototypes for this application. Certain modifications are necessary to accomplish this technology transfer.

2.7.1 Circuit Design

Extensive work has been performed in actual circuit design including some prototypes using components that are known to be available with space qualified ratings and which have known radiation characteristics, assuming that the NPOESS satellite may be exposed to over 100 kRad total radiation doses over the mission lifetime. It was determined which parts of the existing designs for the RPI instrument (a magnetospheric sounder for NASA's IMAGE satellite) or from the ground-based Digisonde sounders could be used directly and which require radically different components or concepts. Those circuits requiring more extensive modification have been bread boarded and tested, and are listed here:

1. Synthesizer with the chirp waveform function
2. 3-Receiver, 12-bit digitizer with additional 32 channels for diagnostic monitoring
3. RF Power Amplifier
4. VME Digital Interface
5. Receiver Preselector
6. RS-422 Serial Interface
7. Antenna Preamplifier

The design of the power conversion circuitry, which was not prototyped, relies heavily on the selection of space qualified DC/DC converters. Samples of three converters were obtained, a clock oscillator circuit was developed to drive the synchronization clock and an EMC filter was developed to suppress switching noise generated inside the converter. Based on measurement data, we can expect these modules to operate with efficiencies around 70 percent. Given these efficiencies and the measured or estimated power consumption per electronics module, Table 1 reflects the spacecraft resource requirements to support a TOPAS instrument.

Table 1. Measurement Results for Interpoint DC/DC Converters

Model MHF2805S								
%Load	Rl	Vo	Io	Po	Vi	Ii	Pi	Effic
103	2	4.98	2.5	12.4	26	.64	16.7	74.3%
70	3	4.99	1.7	8.3	26	.42	11.1	74.9%
40	5.1	5.01	1.0	5	26	.27	7.0	70.1%
MHF2815D								
40	150	30	.2	6	26	.3	7.75	77.4%
MSA2815D								
101	89	15	.17	2.5	26	.27	7.1	71.4%
60	150	15	.1	1.5	26	.18	4.6	64.4%
30	330	15	.045	.68	26	.11	2.8	48.1%

2.7.2 Waveform Development for TOPAS, Topside Advanced Sounder

In order to correctly interpret Doppler aliased echoes from the phase coded pulse signals, the sounder should alternate a chirped pulse waveform with the phase coded pulse waveform when operating in the presence of high Doppler shifts. The high Doppler environment may be caused by spacecraft platform motion and/or by fast plasma drift at high latitudes. For instance, at 10 MHz, with relative motions of 2 km/sec, Doppler shifts received from an ionospheric irregularity that is 30°, off vertical, would be 66 Hz. This Doppler shift will alias if the pulse repetition rate is less than 132 Hz. The echo signal must maintain a constant Doppler shift to allow Doppler integration over several seconds. The phase code also relies on having a small phase shift (e.g. less than 20°) over the duration of each pulse, which limits its useful range to about the same 66 Hz maximum Doppler environment. In contrast, the chirp waveform does not require any coherence in the echo signal for its most basic function (i.e. a single pulse) and due to a higher signal processing gain, this waveform will enable detection of ionospheric features with a single transmitted pulse. When the medium does remain coherent for several pulses (e.g. IPP = 100 msec) the chirp pulse can also provide a Doppler spectrum by using a sequence of repeated chirp pulses similar to an FM/CW Over-the-Horizon radar technique.

In order to provide greater spectrum resolution, the integration period needs to be longer than the coded sequences (1.25 msec rather than 533 μsec). There is a tradeoff between letting the transmitter blank out some of the received echo signal from close ranges, vs. transmitting a longer pulse to enhance the echoes returning from far ranges. Regardless of how long the pulse is, the signal from close-in ranges (those ranges that are already providing an echo at the time the transmitter shuts off) will continue.

The 60 kHz spectrum bandwidth is divided into 256 range bins by the spectrum analysis, but only 30 kHz of that spectrum bandwidth has received signal, so there is a S/N gain of 128 (power), or 21 dB, with *only a single pulse*. The phase-coded waveform using 16 chips and 4 repetitions also provides 21 dB, but takes 8 pulses (4 complementary pairs, i.e., Code 1 followed by Code 2) over a 40 msec period, therefore the chirp pulse provides a gain of 8 in time. The chirp pulse therefore has an advantage in environments where the echoes may not be coherent over long intervals.

Range-Doppler Ambiguity:

Since the range is determined by the frequency difference between transmitted and received signals, any Doppler shift induced on the signal will not be distinguishable from a range delay change. As above, the sensitivity of the range determination to Doppler shift can be computed using the inverse of the sweep rate, 125 nsec/Hz or 18.75 m/Hz. Therefore a 50 Hz Doppler shift would create a 937.5 m range error, which is not detectable by this system. The tradeoff made above allows some broadening of the spectrum content of signals received from the extreme ends of the range window (the truncation and resulting frequency/range broadening also applies to any echoes beyond 620 km) in order to achieve better sensitivity in

the middle of the range profile. The major gain in S/N ratio achieved here is no surprise, since the transmission duty factor is increased from 10 % (16-chirp phase coded pulse) to 40%.

Since shorter pulses result in poorer spectrum resolution after de-chirping (and therefore poorer range resolution) it does no good to stop transmitting before all echoes of interest have started arriving. For example, the first 0.6 msec of a 1.2 msec pulse returned from a range of 90 km (radar range is 150 km/msec) will be blanked out since the transmitter is still on at this time. However, this signal continues to arrive for another 0.6 msec after transmission has ceased and has the frequency shift, relative to the swept frequency (chirped) local oscillator, characteristic of echoes from 150 km. Therefore, the truncated echo produces a 1600 Hz line width in the spectrum analysis for producing the range profile, and therefore has only half the range resolution of a full 1.2 msec pulse. Note however, by shortening the transmission to 0.6 msec to avoid blanking out echoes from close ranges, we would still receive a 0.6 msec pulse, resolvable to 1600 Hz. Therefore, transmitting the longer pulse really has not degraded the systems performance, and actually improves range resolution and sensitivity at the longer ranges.

2.7.3 Proposed Chirp Waveform Parameters

The preferred parameters are a 1.2 msec pulse repeated every 10 msec for the ground based tests (a change to 6.25 msec, or 160 pulses per second is envisioned for the actual topside sounding). The received signal is mixed with the same sweeping LO that created the transmitted signal in which case the difference frequency is determined by the time delay between transmission and reception. The receiver sweep resets to its start frequency (or in some cases some other offset) and starts sweeping immediately after the transmission ceases. The hardware allows the sweep to start at any of four start frequencies (i.e. it need not start where the transmitter sweep started). Sampling of the receiver output should start immediately after the transmission has stopped, making quick recovery of the receiver and rapid damping of the voltages on the antennas important performance parameters. The received range profile is then frequency analyzed by Fourier transform, to detect the frequency offsets of the "de-chirped" received signals. Since the frequency offset is linearly proportional to the time delay of the echo, this spectrum analysis produces a range (time delay) profile. Any complete or truncated arriving echoes are detected as fixed frequency sinusoidal tones, offset from zero frequency by an amount proportional to their range. The following parameters provide the desired range depth and resolution:

Sweep Rate	8 or 16 MHz/sec (long range or short range mode)
Pulse Length	1.20 msec (producing a 20 kHz sweep range starting at the operating frequency)
PRF	100 Hz (provides 1500 km unambiguous range)
Receiver BW	30 kHz
Sampling Rate	60 kHz complex samples/sec
FFT size	256 pts
Record Length	4.266 msec

Spectrum Width of any echo from 1.25 msec to 3 msec=800 Hz
Frequency Resolution (of FFT): 60 kHz/256 pts=234.375 Hz

Using the reciprocal of the sweep rate, 16 MHz/sec, we get 62.5 nsec/Hz, time delay resolution in the spectrum analysis, corresponding to a time delay of 14.65 μsec, or a resolution of 2.2 km/range bin. Given the bandwidth of the 1.25 ms pulse (800 Hz) however, we have to derate the resolution of the Fourier transform by a factor of three (the dechirped pulse will occupy three adjacent range bins) for a range resolution of approximately 6.6 km.

Range Resolution:	6.6 km, over the range window
Maximum Range:	465 km
Minimum Range:	90 km (closer echoes are detectable but will result in increasingly degraded range resolution

2.7.4 Synthesizer Card Design Modifications for Chirp Signal Generation

The DPS Frequency Synthesizer is used for both the transmitter function and receiver function (local oscillator, or LO) and is based on a direct digital synthesizer (DDS) chip produced by Stanford Telecom. When clocking the DDS at 40.96 MHz the third of the six internal DDS control register bytes (Register 3) defines units of 19.53125 Hz (the MSB, Register 5's units are 1.28 MHz). The lower four bits of the next register up (Register 4) can count 0 to 16 units of 5 kHz. To create a sweeping synthesizer frequency, these 12 bits (in Register 3 and 4) are counted up or down by a 12 bit binary counter at a rate of 409.6 kHz, thus creating an 8 MHz/sec sweep rate. Since these 12 bits are counted by hardware, the sweep start frequency can only be set to 80 kHz resolution (the value of the next bit above the "msb" of the counter output). A frequency of 8.1 MHz cannot be synthesized, but only a frequency of 8.08 or 8.16 MHz. With a 30 kHz receiver bandwidth, 80 kHz steps are reasonable. In making a new synthesizer it is advantageous to use a 51.2 MHz clock and then using the 12-bit counter we have 25 kHz steps, a desirable feature for ionograms.

The DPS's synthesizer allows for different frequency sweep start positions, fc-40 kHz, fc-20 kHz, fc+20 kHz, and fc+40 kHz. By loading different presets into the 12-bit counter the sweep can start at one of these four offsets, and sweep at 8 MHz/sec, up or down and continue for any length of time. Nominally, 5 ms is used for transmission and 2.133 or 4.266 ms for reception.

The resolution depends on the Range Sensitivity Factor (RSF), which is proportional to the inverse of the sweep rate. The inverse of the sweep rate specifies the time delay sensitivity that relates the propagation time to the observed frequency offset. Therefore, to find the RSF one only needs to convert the units of msec to units of km (i.e. multiply by c/2). Using the 1192 Hz/sec sweep as an example,

RSF = c/2 * delay sensitivity = (150 Mm/sec) / (16 MHz/sec) = 9.37 m/Hz

With conventional spectrum analysis (Fourier transformation) the 3 dB spectral width of a pulsed sinusoid is the inverse of the pulse width, so the 1.25 ms pulse results in an 800 Hz line in the range spectrum and a range resolution of 7.5 km. Since 256 samples are made at a

sampling rate of 60 kHz the time domain record is 2.133 ms long. Therefore the frequency resolution in the Fourier transform (the width of one frequency bin) is 468 Hz and the received 800 Hz pulse spans 2 spectrum lines. Note however that a non-pulsed (continuous) sinusoid occupies 3 or 4 spectrum lines due to the spreading caused by a Hanning window. Therefore, with either a pulsed or non-pulsed signal, there will be at least 64 resolvable ranges out of the 128 computed in the transform. *Nothing is lost by the fact that the echo doesn't occupy the entire sample window, and the match of signal bandwidth to spectral resolution is nearly ideal.*

2.7.5 Software Modifications to Existing DPS Code Required for a Chirp Waveform

1. Use Waveform Option 2 (previously the single chip 33.3 µsec pulse) in the DPS Program menu for Chirp.
2. Modify the Ipc4.out version of the DSP software, operating on the TMS320C30 DSP Processor card to call a special FFT function for the pulse compression operation if Waveform 2 is selected. The output of this function goes to buffer memory just as it does for PLSCMP, the Complementary Code pulse compression function, allowing the chirp pulse compression to fit neatly into the existing software design.
3. Change order of bytes sent to DDS chip by the assembly language procedure, "OUTPARAMS". For Qualcomm, the computed data structure had the "pref.fine" frequency control byte (76.3 mHz units) going to Register 00, while in the STEL chip these bits go to Register 2 and the most significant bits, the "pref.MHz" byte, go to Register 5 rather than Register 3; due to the STEL being a 48-bit phase accumulator while the Qualcomm is only 32 bits. The lowest two bytes will not be set. The freq-to-byte routine will fill the unmodified DPS preface structure, using pref.fine for the Reg 2 (the .0763 Hz units) byte and pref.wr for the Reg 5 (1.28 MHz units) byte.
4. Make changes to the setting of the frequency control bits by the routine in the C function freq-to-byte, in dpsmain.c. The setting will require the armenu.dps file to be modified for SYN revision H to reflect the presence of the STEL-1173.
5. DPScntl.exe must be modified, in sysclock handler, to set the Chirp bit in the DDS address register (P-bus port 14h). Since this register was formerly used to set the RF amp output filters (the Half Octave Filter, or HOF card), the half octave filters must be bypassed during the chirp waveform testing.
6. If a 16 MHz/sec sweep rate and a 1.25 msec pulse is used, there is no need to change any of the software timing. Changing the R-pulse to 1.4 msec and the XmtrOn signal to 1.25 msec will allow the generation of a new RCW signal which is high all the time except during the coincidence (NAND function) of the R-Pulse and inverse of XmtrOn. When this modified RCW cycles low, the counters on the SYN card will be cleared to zero thus resetting the frequency sweep to its start frequency.
7. Make a new waveform PROM for the XMT card using Waveform 2 (usually a single 33.33 usec pulse). Make XmtrOn 1.25 msec, XmtrEn 1.3 msec. Also change TIM ROM to allow 1.4 msec R-Pulse.

2.7.6 Hardware/Firmware Modifications to DPS Design Required for Chirp Waveform

Data Acquisition Timing: A new waveform PROM was generated for the XMT card using Waveform 2 (usually a single 33 μsec pulse). This PROM also requires a 1.25 msec R-pulse (twenty five-50 msec counts of the Timing ROM). The LO must roll over to the start frequency at the end of the 1.25 msec. It has swept 10 kHz in that time.

The attached ionograms were taken Dec. 22 and Dec. 24,1997 using:

a. Standard 16-chip Complementary code waveform (Figure 11).

b. The "short range" chirp format (1.2 ms chirp pulse 10 kHz bandwidth and sweep rate of 8 MHz/sec) using a Hanning window for chirp pulse compression and incoherent integration of successive pulses (Figure 12).

c. The same "short range" format, but using no Hanning window during pulse compression (note the range leakage) and incoherent averaging of successive pulses (Figure 13).

d. Same as "c" except that the pulse compression processing uses a Hanning window (Figure 14).

Note that the heights are incorrect for both ionograms. For the complementary code, this is caused by stretching the R-pulse (the digital signal which enables the transmitter) out 650 μsec longer than normal (1.4 msec rather than 0.75 msec) to accommodate the longer chirp waveform. Since the fall of the R-pulse triggers the Digitizer, there is a systematic 97.5 km error. We were not concerned with this since the complementary code ionograms were only made for comparison purposes. This can be remedied by implementing a feature of the Timing card which has not been used in years; that is, to offset the Timing EPROM by setting the A15 bit in the Timing Control Latch.

The observed broadening of E-region echoes is predictable and does not apply in the same way to sounding from a satellite at 600 km or higher, where a longer dead range (200 km rather than 90 km) is expected when using the chirp waveform. As an example, an echo at 100 km arrives 667 μsec after the transmitter pulse starts, but since the system is still transmitting for another 533 μsec, much of this echo is not sampled.

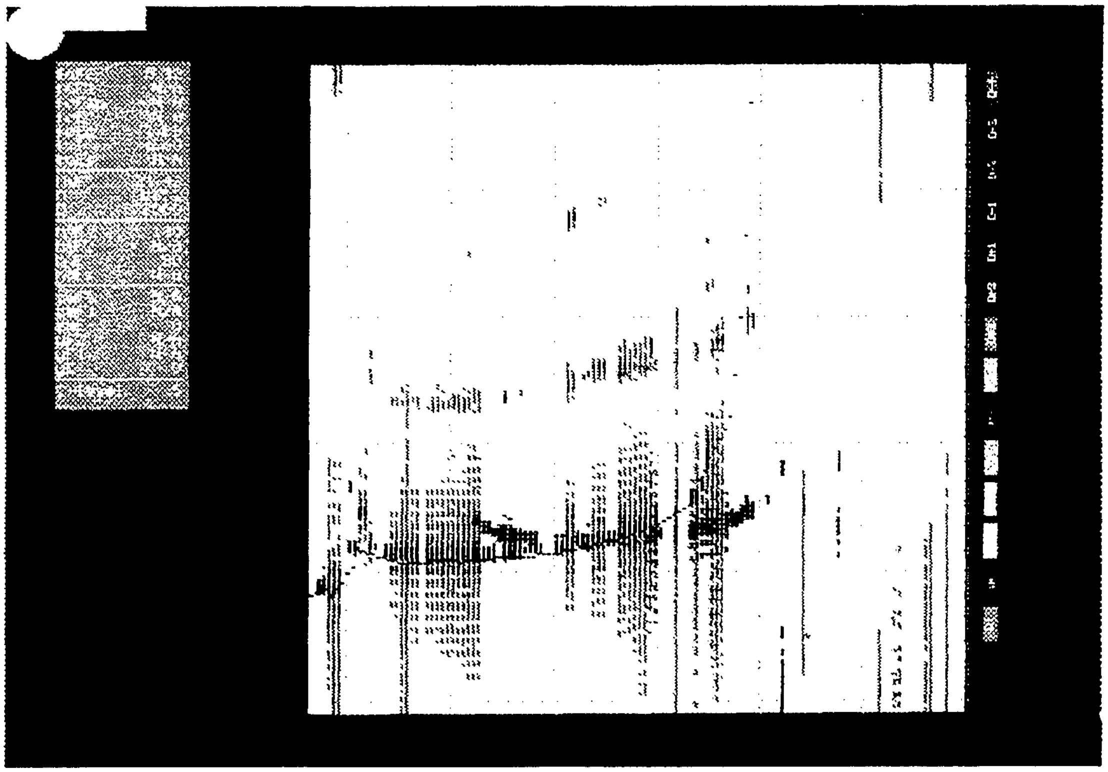

Figure 11. Complementary code ionogram taken as a reference.

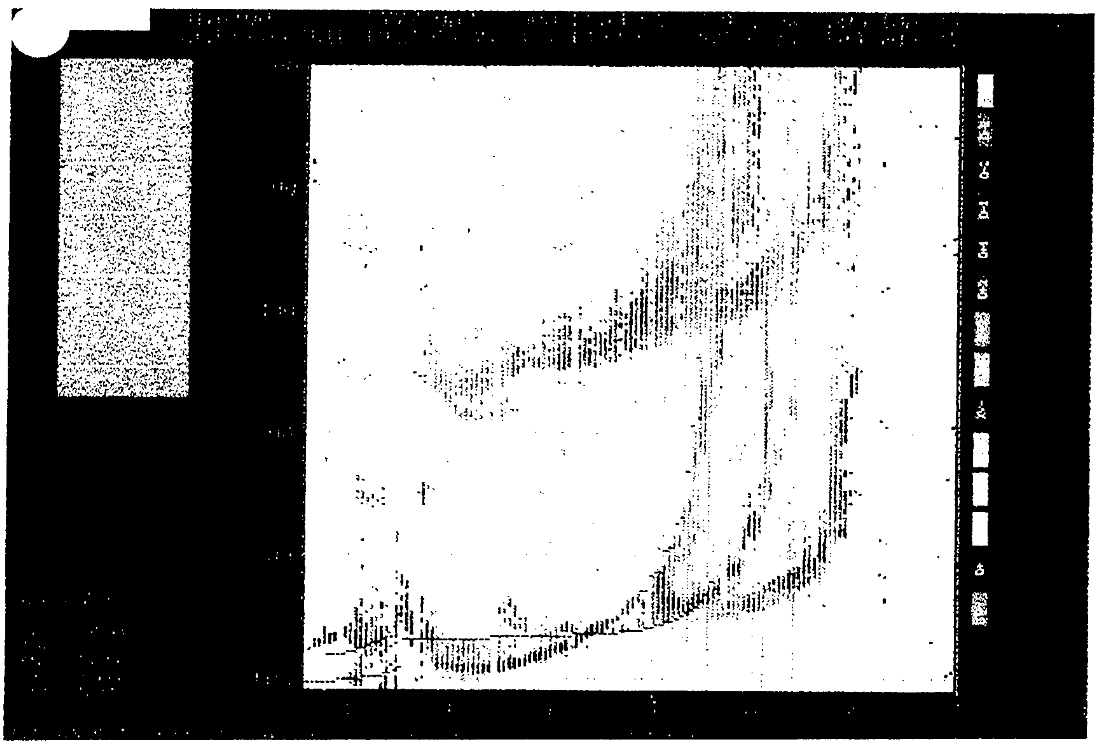

Figure 12. Chirp ionogram using Hanning window and incoherent integration of successive pulses.

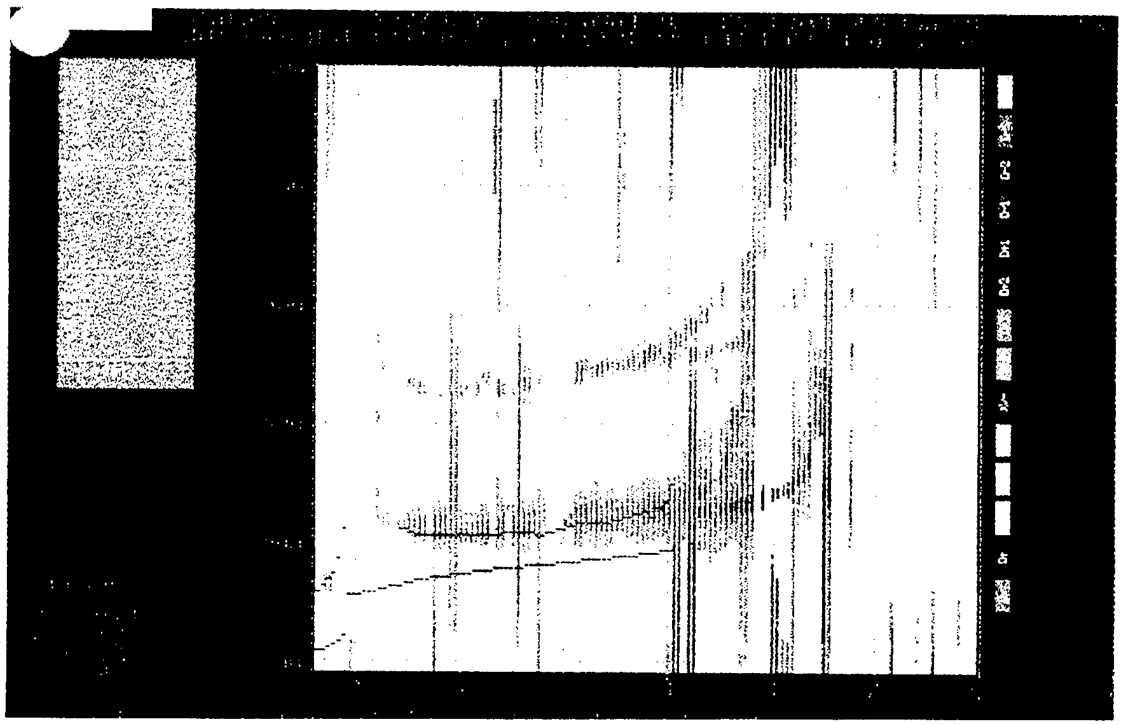

Figure 13. Chirp ionogram, no Hanning window and incoherent integration.

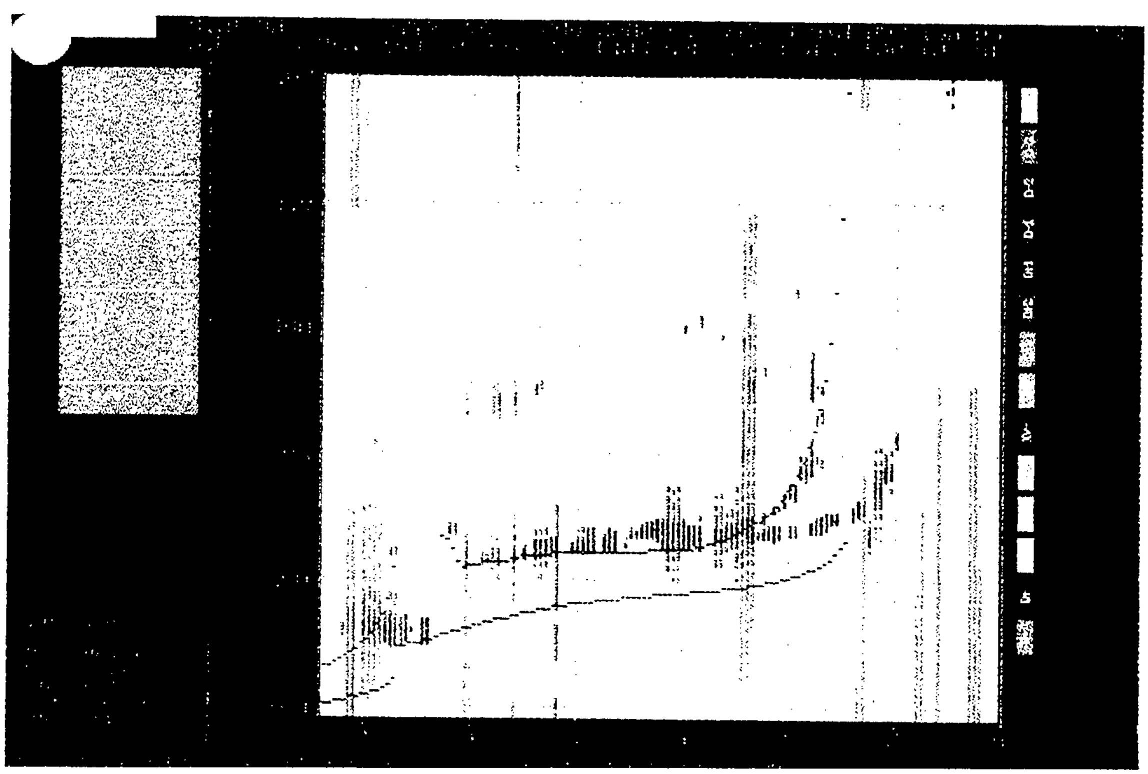

Figure 14. Chirp ionogram using Hanning window and incoherent integration.

The 617 msec that is sampled has an offset frequency of 4664 Hz, i.e. a negative frequency in the sampled data record (since the samples are complex, the negative frequency will be recognized). A 0 Hz offset has been adjusted to appear at 187.5 km, so that -4664 Hz is 20 range bins below at 137.5 km. This is consistent with the observed traces in the trial ionograms.

The noise problem observed in the chirp mode needs to be addressed. The 8 MHz/sec chirp rate means that the 1.2 msec pulse spans 9600 Hz (nominally 10 kHz). The chirp frequency is then reset and the LO starts sweeping again at 1.25 msec. During the receiver sampling time, the LO spans 34 kHz, therefore, since the receiver bandwidth is 30 kHz, a fixed frequency interferer sitting anywhere in the 64 kHz spanning the receive interval will be present in the sampled data record. This interference may cover anywhere from a small part of the receive interval up to nearly all of the 256 samples. If a narrowband interferer is sitting 32 kHz up from the bottom of the receiver pass band at the start of the chirp (fo - 17 kHz), it will be slightly attenuated at the beginning of the record, at full strength during most of the record, then again slightly attenuated at the end of the record. Interferers 32 kHz lower in frequency will be full strength at the beginning of the record, then decay somewhere in the middle of the record. Interferers at higher frequencies, up to 64 kHz above the start of the chirp, do not exist at the beginning of the record and appear somewhere in the middle and finish at full strength. From the observation of the echoes, it is clear that the noise sources are relatively constant amplitude fixed frequency sources such as transmitters in the HF spectrum. To improve the rejection of such interference we tried the following steps:

1. Use a Hanning window with the pulse compression FFT. The vertical stripes (range leakage) are not nearly so visible on the DPS screen that has only 22 dB dynamic range.

2. Use two multiplexed frequencies separated by 40 kHz. The range profiles for the two frequencies should contain signal echoes at approximately the same range. We have allowed for a 5 km range shift, i.e. two range bins, between the two frequencies. However, sources of interference at one frequency are not likely to appear in the other. Since the range is linearly related to the spectrum position, the interference can be in the last half of one range profile and in the first half of the other. This leaves the possibility of piecing together a full range profile from the best two of the four half range profiles, which handles the case of one strong interferer or several closely spaced ones, within 100 kHz.

The chirp is the short-range set of parameters described above (a 1.25 msec pulse chirping over a 20 kHz bandwidth). The chirp pulse compression algorithm uses a rectangular weighting function (i.e. not Hanning weighted) on the time-domain data. Since the pulse compression is done with a Fourier transform, the absence of a weighting function creates a sin(x)/x leakage pattern that is clearly visible above and below the actual echo trace in Figure 13 and 14.

In Figures 12 and 13, the echoes from successive pulses were integrated incoherently, but thresholded to eliminate interference lines). Each echo amplitude was squared (power) and then added to an accumulator, producing an average power for each echo range bin. The

ionograms in Figure 14 used a Hanning window for pulse compression, and also used the standard DPS technique of coherent integration by making a Doppler spectrum at each range.

Therefore the echoes displayed in Figure 14 are the peak Doppler line selected out of an entire Fourier spectrum at each range. Figure 15 shows the effect of using interpulse phase modulation, i.e. inverting the transmitted phase between pulses and then inverting again the received samples. This has the effect of chopping up any coherent interference, such as broadcast station carrier signals as well as internally generated clock and oscillator signals.

2.7.7 Transmitted Power Calculations for 5W TOPAS Transmitters

The TOPAS transmitter has two independent RF power amplifiers to simplify signal distribution and to provide redundancy. Each amplifier drives a maximum of 5 W into each monopole of a 20 m dipole. A tunable series L-C antenna coupler will be used with switched inductors and capacitors. A variable power supply will allow the system to limit the antenna voltage to <3000 V_{rms}. The transmitter power amplifiers and antenna couplers for the two monopoles are mounted at the satellite skin directly driving the monopoles. The self-imposed voltage limit reduces the risk of arcing and component damage.

3. Publications

A number of papers reporting our research were published during the report period:

Scali, J.L., and B.W. Reinisch, Geomagnetic storm time studies using Digisonde data, Adv. Space Res., 20, 9, 1679-1688, 1997.

Reinisch, B.W., D.M. Haines, K. Bibl, I. Galkin, X. Huang, D.F. Kitrosser, G.S. Sales, and J.L. Scali, Ionospheric sounding support of OTH radar, Radio Sci., 32, 4, pp. 1681-1694, 1997.

Mendillo, M., J. Baumgardner, D. Nottingham, J. Aarons, B.W. Reinisch, J.L. Scali, and M. Kelley, Investigations of thermospheric-ionospheric dynamics with 6300-Å images from the Arecibo Observatory, J. Geophys. Res., 102(A4), 7331-7343, 1997.

Reinisch, B.W., Modern Ionosondes, in Modern Ionospheric Science, (Eds. H. Kohl, R. Ruster, and K. Schlegel), European Geophysical Society, 37191 Katlenburg-Lindau, Germany, 440-458, 1996.

Sales, G.S., B. W. Reinisch, J. L. Scali, C. Dozois, T. W. Bullett, E. J. Weber, and P. Ning, Spread-F and the structure of equatorial ionization depletions in the Southern Anomaly Region, J. Geophys. Res., Vol. 101, No. A12, pp. 26,819-26,827, 1996.

Colerico, M., M. Mendillo, D. Nottingham, J. Baumgardner, J. Meriwether, J. Mirick, B.W. Reinisch, J.L. Scali, C.G. Fesen, and M.A. Biondi, Coordinated measurements of F region dynamics related to the thermospheric midnight temperature maximum, J. Geophys. Res., Vol. 101, No. A12, pp. 26,783-26,793, 1996.

Huang, X. and B.W. Reinisch, Vertical electron density profiles from digisonde ionograms. The average representative profile, Annali di Geofisica, Vol. XXXIX, No. 4, pp 751-756, 1996.

Galkin, I.A., B.W. Reinisch, G.A. Osokov, E.G. Zazobina, and S.P. Neshyba, Feedback neural networks for ARTIST ionogram processing, Radio Sci., Vol. 31, No. 5, 1119-1128, 1996.

Huang, X. and B.W. Reinisch, Vertical electron density profiles from the digisonde network, Adv. Space Res., Vol., 18, No. 6, pp. (6) 121-(6)129, 1996.

Reinisch, B.W. and X. Huang, Low latitude digisonde measurements and comparison with IRI, Adv. Space Res., Vol. 18, No. 6, pp. (6) 5-(6) 12, 1996.

Reinisch, B.W. and X. Huang, The F1 region at 170 km, Adv. Space Res., Vol. 18, No. 6, pp. (6) 153-(6) 156, 1996.

4. Summary

Considerable progress has been made in the diverse areas of research covered by this project. From the polar region to the equator, these investigations have improved our understanding of the basic processes and are beginning to generate approaches to solving US Air Force communications and navigation problems.

Near the magnetic equator, this research has uncovered the sources of ionospheric irregularities that are associated with satellite scintillation effects. The ability of the Digisonde to image depletion bands as they drift over a station has established the connection between spread-F as observed on the ionograms with the irregular structure within the depletion bands.

Using a simplified model of the chemistry and dynamics of the F-layer has made it possible to compare the observed 630.0 nm red line emission all sky scanning photometer and theory. This exercise has led to the identification of problems with the HAARP system's calibration and has also made it possible to identify the F-layer differences between active (depletions) and quiet nights. This area of research will be developed considerably in the next year, trying to improve the connection of the depletions with satellite scintillation events.

With the development of GDDA by UMLCAR it has become possible to investigate complex drift processes that occur within the same region. In the polar cap it has become possible to determine the basic structure of the polar convection pattern using this technique. In addition, the drift analysis of relatively small structures within the field of view of the Digisonde such as "polar patches" has been facilitated by this technique. This new drift technique has measured horizontal speeds of 1 km/s and greater at several of the polar stations during the magnetic cloud event.

The connection with negative B_z and the presence of these patches was established and with the Digisonde it was possible to measure the electron density enhancement within these patches. The future effort will try to identify the structure within the patch since they are often associated with increases in satellite scintillation.

An important beginning was made on the problem of separating changes in the measured electron density profiles arising from chemistry (recombination) and vertical transport. The observed vertical movement of a constant electron density contour is a combination of both chemistry and transport. After simulations were carried out, the new technique was applied to Arecibo Digisonde data. These results compared favorably to the ISR measurements made at the same location. Complications at Arecibo involving strong four-hour tidal periods required ad hoc modifications to the neutral atmospheric profiles and it was decided to apply the same technique to the more benign site at Puerto Madryn, Argentina. These results were encouraging and the technique will be pursued next year.

Special efforts were made by UMLCAR to contribute to the standardization of ionosonde data formats. Also extensive data cataloging was made for several stations and CD-ROMs were generated for distribution to the World Data Centers. Considerable data were scaled from several sites to contribute to the ionospheric model verification database. UMLCAR is in the process of developing software and data formats that will allow users (secure and public) access to the data at various Digisonde sites via the Internet. As part of this effort, ARTIST 4 was completed including new computers and multiple Ethernet cards to isolate the Air Force access channels.

A concept and breadboard design of a topside advanced sounder (TOPAS) was developed and demonstrated. A Digisonde Portable Sounder (DPS) was modified to incorporate different wave forms recommended for topside sounding in NPOES.